Calhoun
Institutional Archive of the Naval Postgraduate School

Calhoun: The NPS Institutional Archive

DSpace Repository

Theses and Dissertations | 1. Thesis and Dissertation Collection, all items

1980

An investigation of the reacting and non-reacting flow characteristics of solid fuel ramjets

Scott, Winston Elliott

Monterey, California. Naval Postgraduate School

http://hdl.handle.net/10945/15779

Downloaded from NPS Archive: Calhoun

http://www.nps.edu/library

Calhoun is the Naval Postgraduate School's public access digital repository for research materials and institutional publications created by the NPS community. Calhoun is named for Professor of Mathematics Guy K. Calhoun, NPS's first appointed -- and published -- scholarly author.

Dudley Knox Library / Naval Postgraduate School
411 Dyer Road / 1 University Circle
Monterey, California USA 93943

DUDLEY KNOX LIBRARY
NAVAL POSTGRADUATE SCHOOL
MONTEREY, CALIF 93940

NAVAL POSTGRADUATE SCHOOL
Monterey, California

THESIS

AN INVESTIGATION OF THE REACTING AND
NON-REACTING FLOW CHARACTERISTICS
OF SOLID FUEL RAMJETS

by

Winston Elliott Scott

September 1980

Thesis Advisor: D. W. Netzer

Approved for public release; distribution unlimited

T197443

MONTEREY, CALIF 93940

SECURITY CLASSIFICATION OF THIS PAGE (When Data Entered)

REPORT DOCUMENTATION PAGE

READ INSTRUCTIONS BEFORE COMPLETING FORM

1. REPORT NUMBER

2. GOVT ACCESSION NO.

3. RECIPIENT'S CATALOG NUMBER

4. TITLE (and Subtitle)

AN INVESTIGATION OF THE REACTING AND NON-REACTING FLOW CHARACTERISTICS OF SOLID FUEL RAMJETS

5. TYPE OF REPORT & PERIOD COVERED

Master's thesis; September 1980

6. PERFORMING ORG. REPORT NUMBER

7. AUTHOR(s)

Winston Elliott Scott

8. CONTRACT OR GRANT NUMBER(s)

9. PERFORMING ORGANIZATION NAME AND ADDRESS

Naval Postgraduate School
Monterey, California 93940

10. PROGRAM ELEMENT, PROJECT, TASK AREA & WORK UNIT NUMBERS

N605308WR30053

11. CONTROLLING OFFICE NAME AND ADDRESS

Naval Weapons Center
China Lake, California 93555

12. REPORT DATE

September 1980

13. NUMBER OF PAGES

79

14. MONITORING AGENCY NAME & ADDRESS(if different from Controlling Office)

Naval Postgraduate School
Monterey, California 93940

15. SECURITY CLASS. (of this report)

Unclassified

15a. DECLASSIFICATION/DOWNGRADING SCHEDULE

16. DISTRIBUTION STATEMENT (of this Report)

Approved for public release; distribution unlimited

17. DISTRIBUTION STATEMENT (of the abstract entered in Block 20, if different from Report)

18. SUPPLEMENTARY NOTES

19. KEY WORDS (Continue on reverse side if necessary and identify by block number)

Propulsion, Ramjet, Solid Fuel Ramjet

20. ABSTRACT (Continue on reverse side if necessary and identify by block number)

An investigation was conducted to determine the relationship between the non-reacting and the reacting flow characteristics of solid fuel ramjets. Polymethylmethacrylate fuel grains were burned in a ramjet motor on a thrust stand. Combustion efficiency, regression rate profile and pressures were determined for the reacting flows and compared to profiles obtained in non-reacting flows for velocity, pressure, and near-wall and centerline turbulence intensity. Near-wall turbulence profiles were in agreement

DD FORM 1 JAN 73 1473 EDITION OF 1 NOV 68 IS OBSOLETE
S/N 0102-014-6601

SECURITY CLASSIFICATION OF THIS PAGE (When Data Entered)

20. (continued)

with the fuel regression profiles obtained in reacting flows. Combustion efficiency was found to be a strong function of mixture ratio. Near-wall mixing significantly increased fuel regression rate.

Approved for public release; distribution unlimited

An Investigation of the Reacting and Non-Reacting Flow Characteristics of Solid Fuel Ramjets

by

Winston Elliott Scott
Lieutenant, United States Navy
B.M.Ed., Florida State University, 1972

Submitted in partial fulfillment of the requirements for the degree of

MASTER OF SCIENCE IN AERONAUTICAL ENGINEERING

from the

NAVAL POSTGRADUATE SCHOOL
September 1980

ABSTRACT

An investigation was conducted to determine the relationship between the non-reacting and the reacting flow characteristics of solid fuel ramjets. Polymethylmethacrylate fuel grains were burned in a ramjet motor on a thrust stand. Combustion efficiency, regression rate profile and pressures were determined for the reacting flows and compared to profiles obtained in non-reacting flows for velocity, pressure, and near-wall and centerline turbulence intensity. Near-wall turbulence profiles were in agreement with the fuel regression profiles obtained in reacting flows. Combustion efficiency was found to be a strong function of mixture ratio. Near-wall mixing significantly increased fuel regression rate.

TABLE OF CONTENTS

LIST OF FIGURES

Figure No. Page

LIST OF TABLES

SYMBOLS

A	area
A*	nozzle throat area
A/F	air-fuel flow rate ratio ($\dot{m}_a/\dot{m}_f$)
C_F	thrust coefficient
d	orifice or nozzle diameter
D	pipe diameter
F	thrust
F_a	thermal expansion factor
h_w	differential pressure in inches H_2O at 68° F.
K	product of coefficient of discharge and velocity of approach factor
l	PMM fuel grain length
M	Mach number
M_i	molecular weight of gas constituent i
$\overline{M}$	average molecular weight of the gas
m	mass
$\dot{m}$	mass flow rate
n	moles
P	pressure
P_t	stagnation pressure
R	gas constant
$\overline{R}$	universal gas constant; 1545.43 ft-lbf/R-(lbm-mole)
$\dot{r}$	fuel regression rate
r	radius

t	time
T	static temperature
T_T	stagnation temperature
T_{T_1}	reacting flow stagnation temperature calculated from pressure
T_{T_2}	reacting flow stagnation temperature, calculated from thrust
u_e	nozzle exit flow velocity
V	velocity
V_t	total internal volume of PMM grains
w	weight
Y	expansion factor
$\beta=d/D$	ratio of orifice to pipe deameters
γ	ratio of specific heats
γ_2	air specific weight
$\eta_{\Delta T_P}$	temperature rise efficiency based on pressure
$\eta_{\Delta T_F}$	temperature rise efficiency based on thrust
ρ	density

Subscripts

a	air, ambient conditions
c	chamber
e	nozzle exit
i	initial, species i, probe i
f	final, fuel
t	total (air + fuel)
th	theoretical

ACKNOWLEDGEMENT

I would like to express my appreciation to Prof. David Netzer for his patience and assistance in completing this project. Thanks also to Mr. Pat Hickey for his kindly assistance. Special thanks goes to my wife Marilyn, son Elliott and daughter Megan for their support and understanding during my stay at NPS.

I. INTRODUCTION

As the overall performance demand of tactical weapons increases, the necessary complexity and associated cost of such weapons increases. Much of this complexity and cost is that directly associated with the propulsive system which must be reliable, highly efficient and predictable in performance over a wide range of altitudes and Mach numbers. Evidence exists that indicate solid fuel ramjets (SFRJ) could possibly be a viable alternative to existing counterparts, meeting all of the desirable characteristics stated above. Their relatively simple construction and use of readily available fuel ingredients support the belief that the SFRJ could be a truly cost effective propulsive system.

Solid fuel ramjet performance is currently known to depend on several factors, including air flowrate, method of air introduction (axially, bypass, side dump, etc.), fuel grain chemical composition and curing process, internal grain geometry, inlet step height, and length to diameter ratio. Binn [Ref. 1] sought to relate the non-reacting flow characteristics of velocity and pressure distributions and turbulence level in the solid fuel ramjet motor to the reacting flow characteristics and overall obtainable performance. If the non-reacting flow data could be correlated to the obtainable performance and fuel regression pattern, then the less expensive

non-reacting flow measurements could be used to estimate obtainable performance in new combustor geometries.

Binn began his investigation by making measurements in non-reacting flows within polymethylmethacrylate (PMM) fuel grains of various configurations. Velocity profiles and near-wall and centerline turbulence profiles were then determined. He then made reacting flow experiments which resulted in the determination of fuel regression rate profiles and temperature rise combustion efficiency values based on thrust and based on nozzle stagnation pressure. The results of those non-reacting and reacting flow experiments indicated that the near-wall turbulence intensity in the non-reacting flow could possibly be used to estimate the fuel regression profile.

This report contains the results of an investigation which continued that begun by Binn. In this investigation, reacting flow tests were conducted first, using PMM fuel grains of various internal geometries and using varying methods of air introduction. Upon completion of the reacting flow tests, the PMM grain configurations yielding the highest performance gains (thrust, efficiency, etc.) were selected for non-reacting flow studies. Another factor considered in the selection of fuel grains for non-reacting flow tests was the grain internal geometry. Specifically, how this geometry was believed to affect near-wall and centerline turbulence levels. A side-dump inlet grain configuration was selected for cold flow studies despite the fact that a successful hot firing of this

grain was not initially accomplished. The practicality of the single inlet geometry (axial or side) fostered this selection.

A detailed comparison between the cold and hot flow results was made in an attempt to improve the existing level of understanding of configuration effects on flow and combustion characteristics.

II. METHOD OF INVESTIGATION

The collection of experimental data for this report was begun by selecting several grain configurations for reacting flow testing. This selection process was based primarily on their speculated influence on turbulence intensity distribution within the fuel grain.

The polymethylmethacrylate grain configurations selected were:

1. cylindrically perforated grain (Fig. 1)
2. cylindrically perforated grain with side-dump dome inlet (Fig. 2)
3. cylindrically perforated grain with enlarged inlet diameter (Fig. 3)
4. cylindrically perforated, internally groved grain (Fig. 4)

Photographs of a cylindrically perforated fuel grain and one with circumferential grooves are presented in Figures 5 and 6, respectively.

The cylindrically perforated fuel grains were used as control grains to which all other results could be compared. They were also used in an attempt to identify any differences in performance which might be due to differences in the curing processes associated with the fabrication of the PMM grains.

The cylindrically perforated grain was tested with (a) a 0.5 inch inlet diameter, (b) a 1.5 inch (normal) and a 1.0 inch

(small) diameter aft orifice plate, (c) a 1.0 inch diameter orifice plate located midway in the fuel grain, and (d) a wire screen covering the axial outlet.

Binn [Ref. 1] found that the small diameter rear orifice plate caused relatively large scale oscillations within the entire fuel grain and increased the velocity and size of the recirculation zone within the aft mixing chamber. The small diameter aft orifice plate could increase mixing of the fuel vapor and air within the fuel port, possibly leading to higher performance. For this reason the small diameter orifice plate was installed at the rear of the fuel grain during some reacting flow tests. A one inch diameter orifice was installed at the midpoint of the cylindrically perforated grain during one set of reacting flow tests. This orifice could also increase the velocity and turbulence/mixing level of the air and fuel within the fuel grain prior to the aft mixing chamber, and possibly lead to higher performance of the cylindrically perforated grain.

The wire mesh front screen was used to determine the effects of inlet flow distortion/increased turbulence on performance.

The cylindrically perforated internally grooved grain was examined for its near-wall turbulence producing capability.

To examine the influences of inlet velocity and maximization of fuel loading, large inlet diameter grains were examined with 100% of the inlet air introduced axially. The side dump

configuration also was run with no bypass air as was the internally grooved grain. All other grains were examined using both 100/0 air (no bypass) and 50/50 air (50% of the inlet air bypassed to the aft mixing chamber).

The side-dump dome configuration was used to investigate the effects on performance of the location at which the air-flow is introduced. Of primary importance in examination of the side-dump inlet is the practicality of using one inlet vice two on actual ramjet-powered vehicles. Vehicle configuration often dictates that the single inlet be a side inlet vice say, an axial inlet. The side-dump dome grain configuration was examined for variations of dome length, inlet dump size and mass flow rate. Dome lengths of 0.75 inch and 1.5 inch each were tested with inlet dump diameters of 0.5 inch and 0.836 inch. For each of the combinations possible, reacting flow runs at nominal flow rate (0.2 lbm/sec), low flow rate (0.15 lbm/sec) and high flow rate (0.25 lbm/sec) were attempted in search of the proper combination of dimensions and flow rates to produce sustained burning. An attempt was also made to successfully burn a flat-dome grain configuration; a side-dump grain which had a flat surfaced, recessed head (Fig. 2) instead of the rounded recessed surface comprising the dome.

The data collected during the reacting flow tests consisted of air flow rates, grain internal pressures, weight changes, run and ignition times and thrust. Average fuel regression rates were calculated. The mixture ratio, chamber pressure,

and air temperatures were input into the Naval Weapons Center (NWC) China Lake, Ca., Propellant Evaluation Program (PEPCODE) computer program to obtain the theoretical adiabatic combustion temperature. This temperature was used to calculate temperature rise combustion efficiencies based on thrust and based on nozzle stagnation pressure. From the results of these reacting flow tests, several grain configurations were selected for non-reacting flow tests. These grains were: (a) cylindrically perforated grain (100/0 and 50/50 air), (b) cylindrically perforated grain with wire screen (50/50 air), (c) cylindrically perforated grain with circumferential grooves (100/0 air) and (d) side-dump with flat recessed head.

Nonreacting flow data measurements consisted of static and total pressure values and center-line and near-wall hot-wire anemometer studies. Pressure distributions and velocity profiles were determined for each of the configurations tested. Turbulence intensity data was obtained from hot-wire anemometer tests. This cold flow data allowed characterization of the internal flow fields of the SFRJ motor.

At the conclusion of these non-reacting flow tests, a second set of reacting flow tests were made on these same grains.

III. DESCRIPTION OF APPARATUS

A. RAMJET MOTOR

A schematic drawing of the ramjet is shown in Fig. 7. Illustrated are the main sections of the motor itself. These are the head-end assembly, the step insert section, the fuel grain and the aft mixing chamber.

The head-end assembly contains openings for the introduction of the primary air-flow and ports for introduction of the starting fuel and the igniter torch. During a normal ignition sequence the air-flow rate was set at the desired value before the ignition switch was activated. When the ignition circuit was activated, ethylene gas was introduced into the head end of the grain along with primary air-flow. This mixture was ignited with an oxygen-ethylene torch which issued from the face of the step-inlet. Normally about three seconds of ignition was required for PMM combustion to sustain.

The step insert section was provisioned for variations in inlet diameter. For these experimental runs, 0.5 inch and 0.75 inch inlet diameters were utilized with particular grain configurations (details are given in later sections of this report).

The PMM fuel grain itself, when mounted in the motor, became the mid-body of the ramjet. It was mounted between the head-end assembly and the aft-end assembly (aft mixing

chamber, nozzles etc.). The entire apparatus was held together by four threaded rods and nuts.

The aft mixing chamber was located just to the rear of the fuel grain. It is the chamber where bypass air is introduced into the mass flow from the burning fuel grain. Attached to the aft mixing chamber was a pressure tap which allowed measurement of chamber pressure. Also attached to the aft mixing chamber was the ramjet nozzle. For the reacting flow experiments, a converging nozzle of 0.75 inch diameter was used. Due to the decrease in chamber pressure which resulted from the lack of burning during the non-reacting flow tests, a nozzle diameter of 0.483 inch was used to maintain the chamber pressure at close to the hot-flow values.

The photograph in Fig. 8 displays the ramjet assembly.

B. AIR SUPPLY SYSTEM

A schematic of the ramjet air supply system is shown in Fig. 9. From the compressor, the air flows to a reservoir and is regulated from the reservior to the primary and secondary flow pipes. Air flow rates were measured using A.S.M.E. flow orifices [Ref. 2].

The airflow can be either vented into the atmosphere or vented through the ramjet motor (as in normal operation) by the control of two pneumatically operated valves.

Air flowrate was manually controlled by two sonically choked gate valves (one each in the primary and secondary lines.

Figure 10 presented a photograph of the primary and secondary flow lines and the manual gate valves used for setting the respective flow rates.

C. DATA ACQUISITION SYSTEM

The primary instrumentation used in this investigation consisted of various individual and Scanivalve pressure transducers for measurement of total and static pressures and a strain-gage load cell for measurement of thrust. All transducer outputs were recorded on a Honeywell 1508 Visicorder.

A timing reference signal was provided by feeding a 5 hz signal from a laboratory signal generator to the timing channel of the visicorder. This signal produced timing marks on the visicorder trace which could easily be counted to obtain an accurate measure of elapsed time. A frequency counter was used to monitor the signal generator output to ensure the accuracy and stability of the established signal.

Temperatures from the air flow orifices were measured with thermocouples and recorded on a strip chart physically located next to the primary and secondary airflow lines. Motor air inlet temperature was also measured by a thermocouple mounted in the head-end of the ramjet motor and was also displayed on the temperature strip-chart.

During the sequence of hot firing tests, it was necessary to record the PMM fuel grain weight before and after each run. The weighing was accomplished using a balance scale.

Initial cold-fow tests involved determination of the velocity distribution within the fuel grain. This was done at one axial location at a time, using a seven pronged total-pressure rake. This rake is drawn schematically in Figure 11. Pressures from each rake prong, from the ambient atmosphere and from pressure taps in the fuel grain wall, motor head and aft chamber were fed to a 48-channel Scanivalve. The Scanivalve sequentially read each channel and gave a voltage indication of the pressure (versus chamber pressure) on an integrating microvoltmeter. Voltage indications, of course, were later translated into absolute pressure readings.

A hot-wire anemometer system was used in the determination of the relative centerline and near-wall turbulence intensities. The hot-wire was used in the linear mode and the output rms voltage and averaged dc voltage values were recorded. The rms voltage was measured on an rms meter and the average dc voltage was read on the integrating microvoltmeter. An oscilloscope was used for adjusting the stability of the hot-wire system. The hot-wire probes used were in a straight line configuration for centerline measurements and angled to the wall for near-wall measurements. The probes are shown schematically in Fig. 12.

D. SOFTWARE

Data reduction required the use of the NWC PEPCODE computer program which was run on the IBM-360 computer at the Naval

Postgraduate School. Programs for Texas Instruments TI-59 programmable calculator were utilized extensively for additional speed and ease in data reduction.

IV. EXPERIMENTAL PROCEDURES

A. INITIAL CORRECTIONS

Reference 1 reported large run to run variations in the efficiences calculated from thrust. Also noted was that one possibility for these large variations might be inaccuracies in thrust measurement. In examining the possibilities for thrust measurement inaccuracies, it was noted that the air inlet hoses connecting the primary and secondary airflow pipes to the ramjet motor did not hang in a plane perpendicular to the motor as assumed in Ref. 1. Consequently, any thrust on the motor due to mass flow through these hoses would have a component in the axial (relative to the ramjet) direction. This axial component of thrust was calculated and, though small (0.19 lbf) in magnitude, was nevertheless applied as a correction to each reacting flow experimental run. For a choked, converging nozzle, one-dimensional isentropic ideal thrust is given by

$$F = C_F P_T A^* \tag{1}$$

where

$$C_F = \left[(\gamma+1) \left(\frac{2}{\gamma+1}\right)^{\frac{\gamma}{\gamma-1}} - \frac{P_a}{P_T} \right] \tag{2}$$

A preliminary run using air only (no combustion) produced a thrust F = 6.09 lbf with a chamber pressure of P_T = 37.0 psia. Equation 2 yields C_F = 0.870 and an ideal thrust of F = 5.90 lbf (nozzle d = 0.483 in.). The difference in this ideal thrust value and the actual measured value (assuming negligible losses) is that thrust component due to the air hoses.

$$F = 6.09-5.90 = 0.19 \text{ lbf.}$$

In some tests, multiple ignition attempts were required before combustion was sustained. The weight change due to igniter firing prior to sustained combustion should be subtracted from the initial fuel grain weight if maximum accuracy in regression rate, fuel flow rate and other calculated data is to be obtained. To account for this phenomenon, a series of test firings using only the igniter were made. The weight change during the "igniter on" time and length of "igniter on" time were both recorded. A sequence of five igniter firings gave a total "igniter on" time of t = 16.6 sec. and a total weight loss of 14.0 g. A correction factor ($K = \Delta w/\Delta t = 14.0/16.6 = 0.843$ g/sec) was then applied to all reacting flow tests to yield a more accurate initial fuel grain weight.

B. CALIBRATIONS

Prior to the first test run of each group, each pressure transducer was calibrated over the appropriate range of pressures by use of bottled nitrogen, pressure gauges and the

Visicorder. Pressure values read on the gauges were applied to the transducer being calibrated and the corresponding Visicorder display position was marked and labeled. The thrust transducer was calibrated by applying known weights to the transducer through a pulley system, and again marking the appropriate Visicorder display position.

C. DATA EXTRACTION

Those quantities which remained relatively constant (such as the air orifice differential pressures) were compared directly to the calibration traces for their respective transducers and the numerical values were extracted. Those quantities which varied during the tests (such as thrust, chamber pressure, etc.) gave rise to traces which varied in height above their zero references. In extracting these values, a compensating polar planimeter was used to measure the area of the graph underneath each trace. Dividing this measured area by the measured length of that trace yielded an average trace height. This average height was then compared to the corresponding transducer calibration to determine numerical values.

D. REACTING FLOW EXPERIMENTS

Following transducer calibration, the mass flow rate of air was manually set using the gate valves shown in Fig. 10. The value of mass flow was set by establishing the necessary differential pressure ΔP for the values of P_T, and T at the orifice in question. The equation for mass flow rate used is

given by Ref. 2 as:

$$\dot{m}(\text{lbm/sec}) = [359/3600](K)(d)(F_a)(Y)\sqrt{h_w \gamma_2} \qquad (3)$$

where

$Y = 1 - (0.41+0.35\beta^4)\Delta P/P_T \gamma$

ΔP = orifice pressure drop

$\gamma = 1.4$

γ_2 = P(144)/RT (air specific weight)

β = d/D (orifice diameter/pipe diameter)

$F_a = 1$

$K \approx 0.6047$ (a function of pipe Reynolds number)

h_w = ΔP in inches of H_2O

The value of P_T was set, T was measured and ΔP was varied (using the gate valves) to give the desired $\dot{m}$. Most tests were run at an total mass flow rate of approximately 0.2 lbm/sec.

Each reacting flow test was run for approximately 45 seconds with a typical 3 second ignition time. Following each run, pressure, thrust and timing data was extracted from the Visicorder traces as outlined above. The fuel grain weight change (Δw) was recorded along with temperatures (motor inlet and orifice temperatures), atmospheric pressure P_a, forward and aft end (fuel grain) diameter changes, fuel lot and grain configuration.

Actual mass flow rate was calcualted using equation (3) with the actual values for ΔP and P_T from the Visicorder traces.

Fuel flow rate was calculated using the ratio of fuel grain weight change to run time.

$$\dot{m}_f = \Delta w/\Delta t = (w_i - w_f)/\Delta t = (w_{i_m} - K(\Delta t) - w_f)/\Delta t$$

where the correction factor for weight loss during ignition has been applied.

The weight change of a cylindrically perforated PMM fuel grain was expressed as

$$\Delta w = w_i - w_f = \rho_f g \pi l (d_f^2 - d_i^2)/4$$

and therefore

$$\bar{d}_f = \sqrt{\frac{4\Delta w}{\rho g \pi} + \bar{d}_i^{\,2}}$$

The change in average radius is $\Delta\bar{d}/2 = \bar{d}_f/2 - \bar{d}_i/2 = \Delta\bar{r}$. Average fuel regression rate ($\dot{\bar{r}} = \Delta\bar{r}/\Delta t$) based upon weight loss was then calculated for each test using

$$\dot{\bar{r}} = \frac{1}{2\Delta t}\left\{\sqrt{\frac{4\Delta w}{\rho g \pi} + d_i^2} - d_i\right\} \qquad (5)$$

Regression rate was also calculated based on the change in fuel grain aft end diameter

$$\dot{\bar{r}} = (d_f - d_i)2\Delta t \ . \qquad (6)$$

An error analysis done by Boaz and Netzer [Ref. 3] indicated that $\dot{r}$ based on weight change resulted from an equation with a smaller precentage of uncertainty than equation (6).

Average initial diameter values ($\bar{d}_i$) for the PMM fuel grains with piecewise varying internal geometries were computed. This computation was based on equating the total calculated internal volume V_t to that of an equivalent centrally perforated, constant diameter fuel grain. For example, grain configuration 3 (Fig. 3) yielded:

$$V_t = v_1 + v_2 + v_3$$

$$= \pi \left[\left(\frac{2.248}{2}\right)^2 (4) + \left(\frac{1.8765}{2}\right)^2 (0.743) + \left(\frac{1.505}{2}\right)^2 (7.197) \right]$$

$$= 30.73 \text{ in.}^3$$

Equating this volume to the identical cylindrical volume,

$$V_t = \pi d_i^2 (\ell/4)$$

$$30.73 = \pi (d_i/2)^2 (11.94)$$

Thus

$$\bar{d}_i = \sqrt{\frac{30.73(4)}{\pi(11.94)}} = 1.81 \text{ in.}$$

The use of NWC PEPCODE followed initial data extraction. PEPCODE input data for the PMM-air propellants included the fuel-air ratio, and chamber and ambient pressures. Pertinent PEPCODE output consisted of equilibrium gas composition within

the combustion chamber in moles (n_i), total gas moles n, and theoretical combustion temperature. The average molecular weight of the gas was computed using

$$\bar{M} = \sum_i (n_i/n) M_i \quad .$$

The gas constant $R = \bar{R}/\bar{M}$ was then calculated for each run, where $\bar{R}$ is the universal gas constant.

"Experimental" values of combustor stagnation temperatures were calculated in two ways, one based on pressure and one based on thrust. The one-dimensional continuity equation ($\dot{m} = \rho AV$) was expressed in terms of chamber stagnation properties for the choked nozzle.

$$\dot{m}_t = \frac{P_t A^* \sqrt{g}}{\sqrt{R T_T}} \left[\gamma \left(\frac{2}{\gamma+1} \right)^{\frac{\gamma+1}{\gamma-1}} \right]^{\frac{1}{2}} \tag{7}$$

From this equation T_T was found.

$$T_T = \left[\frac{P_t A^*}{\dot{m}_t} \right]^2 \left\{ \frac{g\gamma}{R} \left(\frac{2}{\gamma+1} \right)^{\frac{\gamma+1}{\gamma-1}} \right\}$$

However, chamber static pressure (P_c) rather than stagnation pressure (P_T), was recorded experimentally. Thus

$$T_{T_1} = \left(\frac{g\gamma}{R} \right) \left[\left(\frac{2}{\gamma+1} \right)^{\frac{\gamma+1}{\gamma-1}} \right] \left[1 + \frac{\gamma-1}{2} M^2 \right]^{\frac{2\gamma}{\gamma-1}} \left[\frac{P_c A^*}{\dot{m}_t} \right]^2 \tag{8}$$

The values of γ and R used in this expression were obtained from the PEPCODE equilibrium combustion calculations. The Mach number M was computed from the isentropic flow relation

$$\frac{A}{A^*} = \frac{1}{M}\left[\frac{1 + (\frac{\gamma-1}{2})M^2}{\frac{\gamma+1}{2}}\right]^{\frac{\gamma+1}{2(\gamma-1)}}$$

using the value of γ from PEPCODE and the actual nozzle contraction ratio of 8.03. This Mach number was typically less than 0.08 so that P_T could be equated to P_c with negligible error.

The thrust equation

$$F = \dot{m}_t u_e + (P_e - P_a)A_e \ ,$$

can also be solved for an "experimental" combustion temperature. Using the one-dimensional isentropic expression for u_e yields for a choked, converging nozzle and $P_T = P_c$,

$$T_{T_2} = \frac{g(\gamma+1)}{2\gamma R}\left[\frac{F + P_a A_e - \frac{P_c A_e}{\left[\frac{\gamma+1}{2}\right]^{\frac{\gamma}{\gamma-1}}}}{\dot{m}_t}\right]^2 \qquad (9)$$

Equations 7, 8, and 9 were solved for each run by software programs written for the TI-59 programmable calculator.

The temperature rise efficiency was computed for each of the "measured" values of total temperature using

$$\eta_{\Delta T} = \frac{(T_{T_1} \text{ or } T_{T_2}) - T_{T_a}}{T_{T_{th}} - T_{T_a}} \qquad (10)$$

E. NON-REACTING FLOW EXPERIMENTS

The non-reacting flow experiments were conducted with the intent of determining the flow velocity profiles and an indication of the relative turbulence intensity distributions within the fuel grains. The probe used for measuring the total pressures within the fuel grains is shown in Fig. 11. Each probe prong was connected via a pneumatic tube to a Scanivalve. Also input to the Scanivalve were the chamber and air inlet pressures. The Scanivalve output was read on a dc digital voltmeter. All pressures were recorded at axial locations corresponding to 2, 4, 6, 8, 10 and 12 inches aft of the forward end of the fuel grain. The Scanivalve transducer was calibrated prior to each experimental session by placing a known pressure on a selected transducer channel (monitored on a mercury manometer), and recording the voltmeter reading. Calculated calibration factors were in in. hg./mv allowing conversion of experimental data in millivolts to pressure in in. hg.

As the probe axial location was changed during data taking, the sign of the near-wall probe pressure (voltage) values was monitored. When the voltage became negative an indication of the location of the flow reattachment point was obtained.

Substituting the definition of Mach number for a perfect gas

$$M = \frac{V}{\sqrt{\gamma g_c RT}} \tag{11}$$

into the equation for total pressure

$$P_T = P\left[1 + \frac{\gamma-1}{2} M^2\right]^{\frac{\gamma}{\gamma-1}} \tag{12}$$

and rearranging, the equation for velocity at probe i was obtained.

$$V_i = \left\{2\left(\frac{\gamma}{\gamma-1}\right) g_c RT\left[\left(\frac{P_{T_1}}{P_i}\right)^{\frac{\gamma-1}{\gamma}} - 1\right]\right\}^{\frac{1}{2}} \tag{13}$$

A TI-59 software program was used to reduce the millivolt raw data from the dc voltmeter, to P, M, and velocity V_i values.

The TSI hot-wire anemometer system was used in the linear mode to obtain an indication of turbulence intensity. Actually, the measured quantity was the rms voltage to dc voltage ratio. These ratios were usually greater than 15% and therefore cannot actually be called turbulence intensity. However, comparison of this ratio (subsequently called "turbulence intensity") for different tests should indicate the relative magnitudes of the turbulence.

V. RESULTS AND DISCUSSION

A. REACTING FLOW EXPERIMENTS

The results of reacting flow experiments are contained in Table I. A total of 53 hot firings were attempted and 20 were successful (combustion sustained). The unsuccessful attempts included (a) the cylindrically perforated fuel grain with a large diameter (0.75 in) step inlet, (b) cylindrically perforated fuel grain with front screen (no bypass) and (c) cylindrically perforated fuel grain with side-dump/dome inlet. Thirty-one attempts to ignite the side-dump configured fuel grains were made with no success. Each attempt represented a different mass flow rate and inlet size combination. In some of the tests the igniter was maintained for a longer than normal period of time (8 to 10 secs) in an attempt to obtain sustained burning. The apparent inability of the side-dump/dome fuel grain to sustain combustion could possibly be due to the relatively low regression rate of PMM material in the dome region. Identical results (no sustained combustion) were obtained by Binn [Ref. 1] for this fuel grain configuration. Table II indicates the side-dump/dome fuel grain variations attempted.

Calculated values of combustion efficiency based on thrust and on pressure were in general agreement with those reported by Binn [Ref. 1]. Regression rate values were also in good

Table I
Results From Reacting Flow Experiments

Test #	1	2	3	4	5	6	7	8	9	10
Config. #	4	1	1***	1	1	3	1	1*	1**	1**
Inlet Size h/D	.33	.33	.33	.33	.33	.33	.33	.33	.33	.33
$\dot{m}_p$ (lbm/sec)	0.197	0.197	0.199	0.195	0.193	0.197	0.082	0.081	0.073	0.111
$\dot{m}_s$ (lbm/sec)	0.0	0.0	0.0	0.0	0.0	0.0	0.073	0.065	0.060	0.109
$\dot{m}_t$ (lbm/sec)	0.221	0.215	0.218	0.212	0.212	0.213	0.164	0.156	0.143	0.232
t_{ig} (sec)	2.2	8.8	3.0	5.0	4.3	15.3	10.2	7.4	25.6	5.3
t_{burn} (sec)	44.8	41.2	38.	50.	42.9	52.5	45.3	44.9	48.7	47.2
$\dot{r}_{wt}$ (in/sec)	0.0077	0.0063	0.0066	0.0059	0.0066	0.0048	0.0034	.0038	.0036	.0044
(A/f)T	8.2	11.1	10.8	11.4	10.3	12.5	17.0	14.7	13.9	18.2
P_4 (psia)	61.4	53.8	52.6	53.5	54.0	52.5	34.0	33.6	33.5	47.5
F(lbf)	27.3	23.9	23.3	23.1	21.5	22.6	11.5	13.2	11.1	19.3
T_{T4_p} (°R)	4049	3276	3038	3289	3399	3177	2267	2437	2894	2218
T_{T4_F} (°R)	3978	3510	3288	3301	2658	3188	1895	2965	2403	2034
$T_{T4_{th}}$ (°R)	4160	3580	3695	3522	3723	3341	2713	2994	3100	2584
$\eta_{\Delta T_P}$	97.0	90.1	79.3	92.2	89.9	94.2	79.7	77.5	92.0	82.3
$\eta_{\Delta T_F}$	95.0	97.7	87.2	92.7	66.8	94.6	62.8	98.8	73.0	73.4

* 1" Diameter Aft Plate
** Front Screen
*** 1" Diameter Midgrain Plate

Table I (continued)
Results From Reacting Flow Experiment

Test #	11	12	13	14	15	16	17	18	19	20
Config. #	1	1*	1*	1***	1*	1	3	1**	4	1
Inlet Size h/D	.33	.33	.33	.33	.33	.33	.33	.33	.33	.33
$\dot{m}_p$ (lbm/sec)	0.112	0.112	0.193	0.181	0.189	0.19	0.196	0.121	0.186	0.191
$\dot{m}_s$ (lbm/sec)	0.110	0.108	0.0	0.0	0.0	0.0	0.0	0.127	0.0	0.0
$\dot{m}_t$ (lbm/sec)	0.235	0.234	0.212	0.20	0.207	0.211	0.210	0.261	0.210	0.208
t_{ig} (sec)	7.4	10.2	1.0	4.6	4.7	2.6	2.9	3.0	2.3	2.8
t_{burn} (sec)	45.9	46.2	46	47	45.2	44.1	52	45.7	46	46.5
$\dot{r}_{wt}$ (in/sec)	.0046	.0049	.0065	.0065	.0064	.0073	.0037	.0048	.0075	.0062
(A/f)T	17.0	15.6	10.2	9.5	10.5	8.9	14.2	19.1	7.8	11.2
P_4 (psia)	47.9	50.1	51.0	52.0	52.0	53.5	47.3	54.2	58.7	54.8
F(lbf)	20.3	21.2	---	21.0	21.7	22.6	18.7	22.1	24.2	22.3
T_{T4_P} (°R)	2196	2419	3013	3512	3266	3324	2674	2282	3665	3083
T_{T4_F} (°R)	2247	2385	---	2986	3079	3124	2320	1900	3519	3411
$T_{T4_{th}}$ (°R)	2706	2857	3766	3906	3694	4038	3052	2518	4158	3542
$\eta_{\Delta T_P}$	76.6	81.3	76.8	88.4	86.5	79.7	85.1	88.2	86.4	84.8
$\eta_{\Delta T_F}$	79.0	79.8	---	72.8	80.6	74.0	71.1	69.0	82.4	95.7

*1 " Diameter Aft Plate

** Front Screen

*** 1" Diameter Midgrain Plate

agreement with those calculated by Binn, and by Boaz and Netzer [Ref. 3]. The calculated combustion efficiencies based on pressure were much more uniform from run to run than those calculated based on thrust. These differences in calculated efficiencies were probably due to the nature of the total temperature equations (8) and (9). Equation (8) illustrates the dependence of calculated combustion temperature (T_{T_1}) on the square of the chamber pressure-exit area product. Equation (9) shows the temperature (T_{T_2}) dependence on the square of the difference between thrust (F) and the chamber pressure-exit area product. Variations in T_{T_1} values from run to run could be the result of errors in measuring chamber pressure and/or measuring and establishing mass flow rate $\dot{m}_t$. Variations in T_{T_2} values from run to run could be the result of errors in measuring thrust, measuring chamber pressure P_c and/or measuring and establishing $\dot{m}_t$. The square of the difference in the two numerator terms in equation (9) causes relatively large variations in T_{T_2} for small variations in the difference quantitites.

The peak-to-peak amplitude of combustion pressure oscillations were typically less than 3% for the non-bypass condition (also true for the circumferentially grooved fuel grain). All tests with bypass had significantly greater pressure oscillations. The frequency and/or amplitude could not be determined precisely because of the recording speed and the line length connecting the motor to the pressure transducers. In

similar tests, Mady [Ref. 4] reports the frequency to be about 150 hz and the amplitude approximately 20% of chamber pressure in the bypass configuration. The magnitude of the oscillations observed in the present tests were approximately 10% of the chamber pressure. The behavior appears to be linked to the interaction of the bypass air with the shear layer exiting the fuel grain.

1. Cylindrically Perforated Fuel Grain Without Bypass

Table III contains the combustion efficiencies of the tests on the cylindrically perforated fuel grains. It shows that the $\eta_{\Delta T_P}$ values are much more uniform from run to run than are the $\eta_{\Delta T_F}$ values. Bypass generally decreased combustion efficiency for fixed fuel grain lengths and total air flow rate. This results from the high overall air-fuel ratios and inadequate burning in the aft mixing chamber. This behavior was in agreement with the results presented in Ref. 1. It is interesting to note that the air-fuel ratios of tests 7 and 11 were identical despite the fact that the regression rates were somewhat different. The regression rate of test 7 was lower due to the lower air flowrate, but the air-fuel ratios remained the same as did the combustion efficiencies based on pressure. The other calculated combustion efficiencies based on pressure were between 79.7% and 92.2%. The calculated combustion efficiencies based on pressure for test 2, 4 and 5 were all similar in value (88.9% - 92.2%). Test 16 resulted in an unusually high fuel regression rate with a corresponding

TABLE II

Air Flowrate-Inlet Size Combinations
For Cylindrically Perforated Fuel Grain
With Side-Dump/Dome Inlet (Fig. 2)

D_a(in)	0.836	0.5	
L_d(in)	0.75	1.5	
$\dot{m}$ (lbm/sec)	0.15	0.20	0.25

TABLE III

Performance Summary for Cylindrically
Perforated Fuel Grain

Test No.	Comment	$\eta_{\Delta T_F}$	$\eta_{\Delta T_P}$	$\dot{r}$ (in/sec)	A/F
2	Old fuel lot	97.7	90.1	.0063	11.11
4		92.7	92.2	.0059	11.36
5		66.8	89.9	.00656	10.31
7	Bypass	62.8	79.7	.0034	16.95
11	Bypass	79.0	76.6	.0046	16.95
16		74.0	79.7	.0073	8.93
20		95.7	84.8	.0062	11.24

air-fuel ratio near stoichiometric (stoichiometric is 8.33). However, the efficiency was quite low. This behavior is not understood at this time. The differences in fuel grains caused by the curing process could possibly account for some of the differences in regression rate, air-fuel ratio and combustion efficiency. The fuel grains used in tests 16 and 20 were both from a new fuel lot.

The calculated average regression rates are also quite uniform, having a typical value of 0.006 in/sec. This closely corresponds to the results of work accomplished by Binn. There was also close correlation of the calculated regression rates to those computed using the empirical regression rate equation of Boaz and Netzer [Ref. 3]. The regression profiles were also characteristic, increasing from the head-end to a maximum and then decreasing.

2. Cylindrically Perforated Fuel Grain With Midgrain Orifice Plate

Two reacting flow experiments were conducted using this fuel grain configuration. The test results are in Table IV. Run 14 resulted in an air-fuel ratio closer to stoichiometric and had a correspondingly higher combustion efficiency $\eta_{\Delta T_P}$. The regression profiles for these grains were significantly different; with high regression rates near the orifice plate. The apparent large increase in bulk mixing within the fuel grain, however, did not increase the average regression rate or the combustion efficiency compared to the standard grain configuration.

3. Cylindrically Perforated Fuel Grain With Aft Orifice Plate

Table V contains the combustion efficiency data obtained when a one-inch diameter aft orifice plate was installed. The use of bypass resulted in generally lower efficiencies. Bypass results were very similar to those obtained without the small aft orifice plate. Without bypass $\eta_{\Delta T_P}$ also did not vary significantly from that obtained without the plate. Thus, increased bulk mixing within the aft end of the fuel grain did not greatly alter the combustion behavior.

Binn [Ref. 1] reported that the aft orifice plate caused combustion oscillations to occur periodically (approximately every 6 seconds) for short periods of time. This phenomenon showed up as small peaks in pressure/thrust-time traces in Binn's experiments but was not observed in this investigation.

4. Cylindrically Perforated Fuel Grains With Enlarged Inlet Diameters

Table VI contains the results of the reacting flow experiments on the fuel grains with enlarged inlet diameters. The difference between the two enlarged inlet diameter grains was the axial length of the enlarged inlet (Fig. 3.) Cold flow velocity profiles were not measured for these fuel grains but they result in decreased air inlet velocity. The velocity will then increase at the contraction point of 4 or 6 inches. In the 4 inch deep enlarged inlet diameter fuel grain, the high velocity air acts over a longer portion of the

TABLE IV

Performance Summary For Cylindrically Perforated Fuel Grain With Midgrain Orifice Plate

Test No.	Comment	$\eta_{\Delta T_F}$	$\eta_{\Delta T_P}$	$\dot{r}$ (in/sec)	A/F
3	Old fuel lot	87.2	79.3	.00658	10.76
14		72.8	88.4	.0065	9.52

TABLE V

Performance Summary For Cylindrically Perforated Fuel Grain With Aft Orifice Plate

Test No.	Comment	$\eta_{\Delta T_F}$	$\eta_{\Delta T_P}$	$\dot{r}$ (in/sec)	A/F
8	Bypass	98.8	77.5	.0038	14.7
12	Bypass	79.8	81.3	.0049	15.63
13		---	76.8	.00654	10.16
15		80.6	86.5	.0064	10.53

fuel grain interior. Turbulence intensity near the wall was probably higher, resulting in a higher regression rate (test 6). The air-fuel ratio in test 6 was lower than test 17 (6 inch deep inlet) and resulted in more nearly stoichiometric combustion and higher efficiency. The fuel regression rates from these tests were generally lower than those for the cylindrically perforated fuel grain. The relatively high combustion efficiencies obtained may be somewhat misleading since large amplitude pressure oscillations were present.

The inlet diameter of the fuel grain of test 6 was enlarged for a length slightly less than that of the upstream end of the recirculation zone. In this test, small amplitude (3% of P_c) oscillations transitioned to large (10% of P_c) amplitude oscillations after 20 seconds of burn time. When the enlarged diameter was lengthened to the downstream end of the recirculation zone, the pressure oscillations began at a low amplitude (5% of P_c) and increased gradually (to 10% of P_c) until shutdown. This behavior appears similar to that observed with bypass; when the reacting shear layer is disturbed it can couple with the resonant frequencies of the ramjet geometry.

5. Cylindrically Perforated Fuel Grain With Inlet Screen

Table VII contains reacting flow tests results for the cylindrically perforated fuel grain with inlet screen. Four test attempts were made with success achieved in three of them. The no-bypass configuration would not sustain

combustion. In cold flow tests, the screen was observed to significantly increase the centerline turbulence intensity. As noted by Binn [Ref. 1], "this amount of turbulence greatly affected the mass transport of air into the recirculation region. This could possibly cause the normally fuel rich recirculation zone to be saturated with air, thereby quenching the combustion reaction. The reduction of air inlet velocity (mean and fluctuating components) with the use of bypass was apparently enough to allow the flameholder to sustain combustion in the fuel grain." Combustion was attained for each case involving 50% bypass.

The higher efficiency obtained in test 9 ($\eta_{\Delta T_P}$) resulted from the lower than nominal air mass flowrate with a mixture ratio corresponding closer to stoichiometric.

The regression rate of this fuel grain configuration was generally lower than that of the standard cylindrically perforated fuel grain. The corresponding combustion efficiencies were very close to those of the cylindrically perforated grain.

6. Cylindrically Perforated Fuel Grain With Circumferential Grooves

Reacting flow tests on the cylindrically perforated fuel grain with circumferential grooves produced the results in Table VIII.

This fuel grain geometry resulted in a relatively large regression rate, due apparently to the increased near-wall turbulence intensity caused by the grooved geometry of

TABLE VI

Performance Summary For Cylindrically Perforated Fuel Grains With Enlarged Inlet Diameters

Test No.	$\eta_{\Delta T_F}$	$\eta_{\Delta T_P}$	r(in/sec)	A/F
6	94.6	94.2	.00479	12.5
17	71.1	85.1	.00374	14.2

TABLE VII

Performance Summary For Cylindrically Perforated Fuel Grain With Inlet Screen

Test No.	Comment	$\eta_{\Delta T_F}$	$\eta_{\Delta T_P}$	r(in/sec)	A/F
9	Bypass	73	92.0	.0036	13.9
10	Bypass	73.4	82.3	.0044	18.18
18	Bypass	69.0	88.2	.00484	19.08

TABLE VIII

Performance Summary For Cylindrically Perforated Fuel Grains With Circumferential Grooves

Test No.	$\eta_{\Delta T_F}$	$\eta_{\Delta T_P}$	r(in/sec)	A/F
1	95	97	.00774	8.20
19	82	86	.0075	7.75

its interior. Combustion efficiency was very high when the mixture was only slightly fuel rich (test 1). However, when the increased regression rate resulted in a significantly rich condition, the efficiency decreased (test 21).

A photograph of the fuel regression pattern is presented in Fig. 13. A photograph of a typical motor firing is presented in Fig. 14.

B. NON-REACTING FLOW EXPERIMENTS

Non-reacting flow experiments were performed on the (a) cylindrically perforated fuel grain, (b) cylindrically perforated fuel grain with inlet screen, (c) cylindrically perforated fuel grain with circumferential grooves and (d) cylindrically perforated fuel grain with side-dump/dome inlet. These tests resulted in velocity profiles and "turbulence intensity" profiles for centerline and near-wall positions inside the fuel grain. Although regression rate profiles are a result of the reacting flow environment, they are discussed here in an attempt to established their relationship to the non-reacting flow experimental results.

Velocity profiles were in very close agreement with those obtained by Binn for corresponding fuel grains. "Turbulence intensity" profiles were generally higher in magnitude than those obtained by Binn though the distribution was nearly the same. The difference in magnitude is thought to be due to differences in methods of air introduction. Binn

introduced air into the ramjet motor inlet axially, whereas the motor configuration used in these experiments (mounted on the thrust stand) required air introduction from opposing sides of the motor head assembly, then turning the air to the axial direction.

All grain configurations used the small diameter inlet (h/D = 0.33), therefore any noted variations in reattachment point location were the result of changes in other quantities (such as bypass).

Measurements were not made within the aft mixing chamber but were confined to within the fuel grain itself.

1. Cylindrically Perforated Fuel Grain Without Bypass

Velocity profiles for this cylindrically perforated grain are drawn in Fig. 15. These profiles are in very close agreement with those reported in Refs. 1 and 5. As can be seen, the air entered the grain at relatively high velocity. At the 2 inch axial location, air velocity was approximately 389 ft/sec at the center of the grain. The profiles became almost uniform at the 8 inch position with magnitudes between 57 and 63 ft/sec. The reattachment point was found to be at approximately 4.8 inches for this grain configuration. Binn [Ref. 1] and Phaneuf and Netzer [Ref. 5] reported the reattachment point location between 3.5 and 5 inches.

Figures 16 and 17 show the "turbulence intensities" for this fuel grain. Maximum centerline "turbulence intensity" occurred at approximately 6 inches and maximum near-wall

"turbulence intensity" occurred at approximately 5 inches. Near-wall "turbulence intensity" was found to have a generally higher magnitude than that at the centerline position, expecially near the entrance to the grain (2 to 3 inches). The "turbulence intensity" profiles closely resembled those of Ref. 1, but with a uniformly higher magnitude.

Figure 18 shows regression rate profiles for three of the grain configurations tested in the cold flow experiments. The curve for the cylindrically perforated fuel grain indicates the location of the maximum regression rate was at approximately 5 inches. This location coincides with the location of maximum near-wall "turbulence intensity" (5 inches) and the location of the reattachment point (4.8 inches).

2. Cylindrically Perforated Fuel Grain With Bypass

Figure 19 shows the velocity profiles for the cylindrically perforated grain with bypass. The velocity profiles were very similar to those for the same grain shape without bypass. The velocity values near the inlet to the grain were lower than those for the no-bypass case, due to the lower flowrate. The velocity at the grain centerline was approximately 195 ft/sec at the 2 inch position and decreased to approximately 31 ft/sec at the 8 inch position, where the overall velocity profile was relatively flat. These profiles very closely resembled those of Ref. 1. Reattachment occurred at approximately 4.3 inches. This is very close to the reattachment point for the no-bypass condition (4.8 inches).

The regression rate reached its peak value at approximately 5 inches, as it did for the no-bypass case. The regression rate profile for the bypass grain, however, varied less than those for the no-bypass grain at axial distances ahead of and behind the reattachment point. Thus, the introduction of bypass air did not appear to effect the location or relative magnitude of the peak regression rate. This result agrees with the behavior of near-wall turbulence profile reported in Ref. 1.

3. Cylindrically Perforated Fuel Grain With Circumferential Grooves

The velocity profiles for the circumferentially grooved grain are shown in Fig. 20. These profiles were not significantly different from those for the bypass and no-bypass cylindrically perforated fuel grain. The flow entered the grain with velocities on the order to 300 ft/sec and became uniform across the grain by the 8 inch position. The reattachment point for this fuel grain was located at approximately 5.1 inches. This was very close to the reattachment point location for the bypass and no-bypass cylindrically perforated fuel grains.

Maximum centerline "turbulence intensity" (Fig. 16) occurred at approximately 8 inches. The "turbulence intensity" began at approximately 20% and increased steadily to its maximum value of approximately 58%. This peak value was located significantly downstream from the peak value which occurred in the non-grooved fuel grain.

The near-wall "turbulence intensity" of the circumferentially grooved grain is depicted in Fig. 17. It was 30% higher than the centerline "turbulence intensity" at the 2 inch location but the maximum value (75%) occurred at approximately the same axial position as it did without the grooves.

The regression rate profile of this fuel grain configuration is drawn in Fig. 18. The maximum regression rate occurred at approximately 5 inches, unchanged from the results of tests on the non-grooved fuel grains. Again, near-wall "turbulence" profiles followed the regression rate behavior. The grooves did significantly increase the average fuel regression rate.

4. Cylindrically Perforated Fuel Grain With Inlet Screen and Bypass

The velocity profiles for the cylindrically perforated fuel grain with inlet screen (bypass) are displayed in Fig. 21. The velocity near the front of the grain was relatively uniform (59 to 67 ft/sec) at positions away from the center of the fuel grain, and relatively higher (135 ft/sec) at the centerline of the fuel grain. Apparently, the high centerline turbulence caused by the inlet screen was sufficient to cause a velocity distribution of this shape. This profile (2 inch location) rapidly began to flatten downstream, and was very uniform by the 6 inch position. The overall magnitudes of the velocities were relatively low when compared to the no-bypass fuel grain tests, but were generally the same as those for the bypass tests with no inlet screen. Reattachment

occurred at approximately 4.3 inches, as for the bypass condition without the inlet screen.

The centerline "turbulence intensity" increased very rapidly from approximately 33% at the 2 inch axial position to approximately 90% at the 5 inch position (Fig. 16). The peak centerline "turbulence intensity" occurred somewhere towards the aft end of the fuel grain as it did in the case of the circumferentially grooved grain (no bypass).

The near-wall "turbulence intensity" (Fig. 17) also increased very rapidly (from approximately 44% at the 2 inch position, to approximately 70% at the 4 inch position) and then decayed. This near-wall "turbulence intensity" profile peaked farther upstream than did the centerline "turbulence intensity."

The regression rate profiles for this fuel grain configuration are depicted in Fig. 18. The peak regression rate occurred near the front of the fuel grain at approximately the 3 inch position. The inlet screen shifted the positions of both the peak regression rate and the near-wall "turbulence intensity" upstream.

5. Cylindrically Perforated Fuel Grain With Side-Dump/Dome Inlet

The velocity profiles for the side-dump inlet configured fuel grain are shown in Figs. 22 and 23. Experiments were made with the total pressure rake both in-plane and perpendicular to the incoming flow.

The velocity profiles show that the velocity distribution was quite symmetric and uniform, even at axial positions near the entrance to the fuel grain. The profiles were relatively flat at the 2 inch axial position and remained so throughout the fuel grain lengths. These profiles are in contrast to those obtained by Binn, were large fluctuations in the mean velocity occurred [Ref. 1, Figs. 20 and 30]. Unlike the results of Ref. 1, large regions of reverse flow did not occur. This is probably due to the single inlet used in this investigation, vice the two opposing side inlets used by Binn.

Turbulence intensity profiles for this fuel grain configuration were not obtained. Due to lack of sustained combustion, regression rate profiles were not available.

VI. CONCLUSIONS AND RECOMMENDATIONS

The fuel grains tested in this investigation were all selected because of the anticipated effect of their respective configurations on near-wall turbulence intensity. Each configuration did affect near-wall turbulence intensity in a portion or in all of the fuel grain length. Most of the calculated combustion efficiencies, however, did not vary significantly from that of the standard cylindrically perforated fuel grain. Combustion efficiency appeared to be a strong function of mixture ratio with a maximum occurring near stoichiometric.

The results of these tests indicate that an increase in near-wall turbulence intensity does increase fuel grain regression rate and mixing; affecting combustion efficiency, depending upon the value of the air-fuel ratio compared to the stoichiometric value. For air-fuel ratios larger than stoichiometric (fuel lean), increased near-wall turbulence intensity can cause increased regression rate, thereby causing the air-fuel ratio to decrease (more fuel) toward stoichiometric. For PMM/air this effect significantly increased the combustion efficiency. Peaks in combustion efficiency for this fuel appeared to occur near stoichiometric.

If the air-fuel ratio is "too large" i.e. very lean, insufficient fuel is present and the relatively large airflow

will tend to quench combustion and lower combustion efficiency. If the air-fuel ratio is less than stoichiometric (fuel rich), then any increase in mixing could result in higher regression rates and cause an even more fuel rich condition. In this investigation, the fuel rich condition decreased combustion efficiency below that obtained near stoichiometric.

The regression rate profiles of PMM fuel grains were found to follow the behavior of the near-wall turbulence intensity profiles and not the centerline turbulence intensity profile. Locations of fuel grain maximum regression rates were always at or near the location of maximum near-wall turbulence intensity.

A question that remains, though, is whether or not the combustion efficiency can be practically controlled by increased near-wall turbulence/mixing. The dependence of combustion efficiency on fuel-air ratio may be much stronger. An investigation should be conducted, in which cylindrically perforated grains of varying lengths (producing air-fuel ratios ranging from relatively lean to relatively rich) are hot fired. Combustion efficiencies of these fuel grains should be compared to the combustion efficiencies of a collection of circumferentially grooved grains (or other near-wall mixing method), also of varying lengths. If the results of these tests indicate that the near-wall mixing is beneficial, then the fuel grain geometry could be optimized. The groove width and depth could be varied in a set of experiments to yield the geometry for optimum performance.

It remains to be determined if and how the PMM curing process affects the combustion properties of the fuel grains. The current work being done in the investigation of fuel properties should be continued.

It is recommended that investigations of the combustion in cylindrically perforated fuel grains with side-dump/dome be continued. Perhaps the use of a fuel with higher regression rate in the dome region would result in flame stabilization.

It is also recommended that additional testing be accomplished to resolve the anomalies between combustion efficiencies based on thrust and based on pressure.

The execution of these recommendations should foster progress in developing the methods of estimating solid fuel ramjet performance from cold flow data.

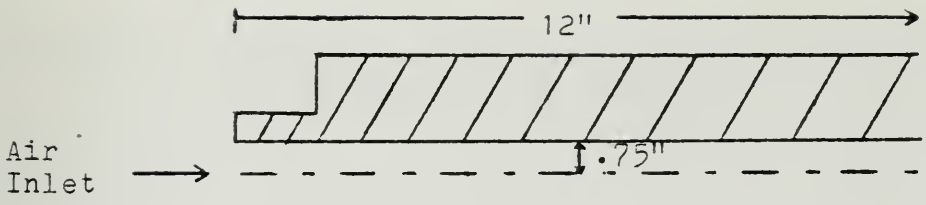

Figure 1. Schematic of Cylindrically Perforated Fuel Grain

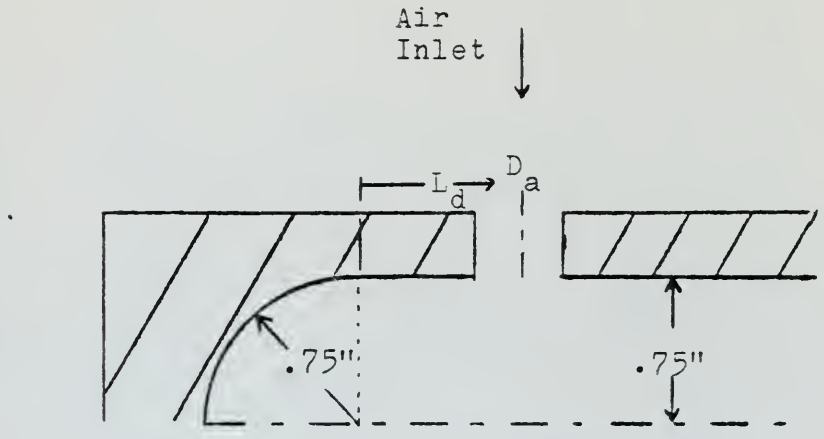

Figure 2. Schematic of Cylindrically Perforated Fuel Grain With Side-Dump/Dome Inlet

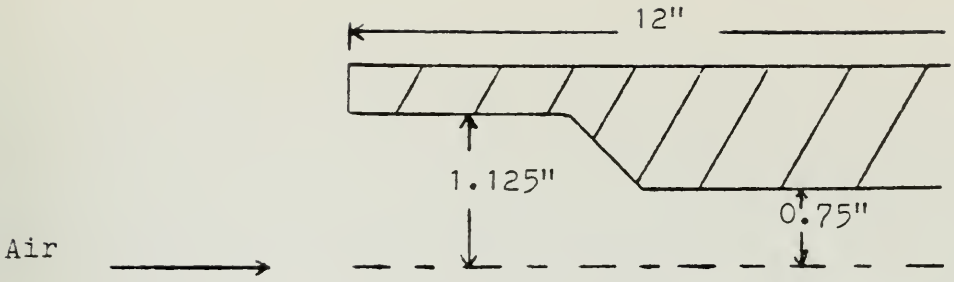

Figure 3. Schematic of Cylindrically Perforated Fuel Grain With Enlarged Inlet Diameter

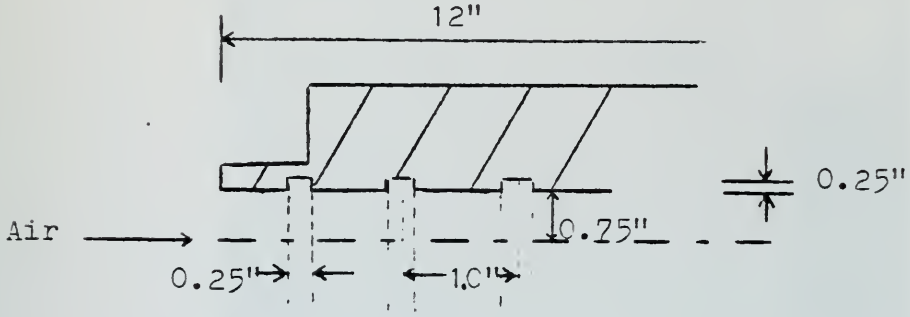

Figure 4. Schematic of Cylindrically Perforated Fuel Grain With Circumferential Grooves

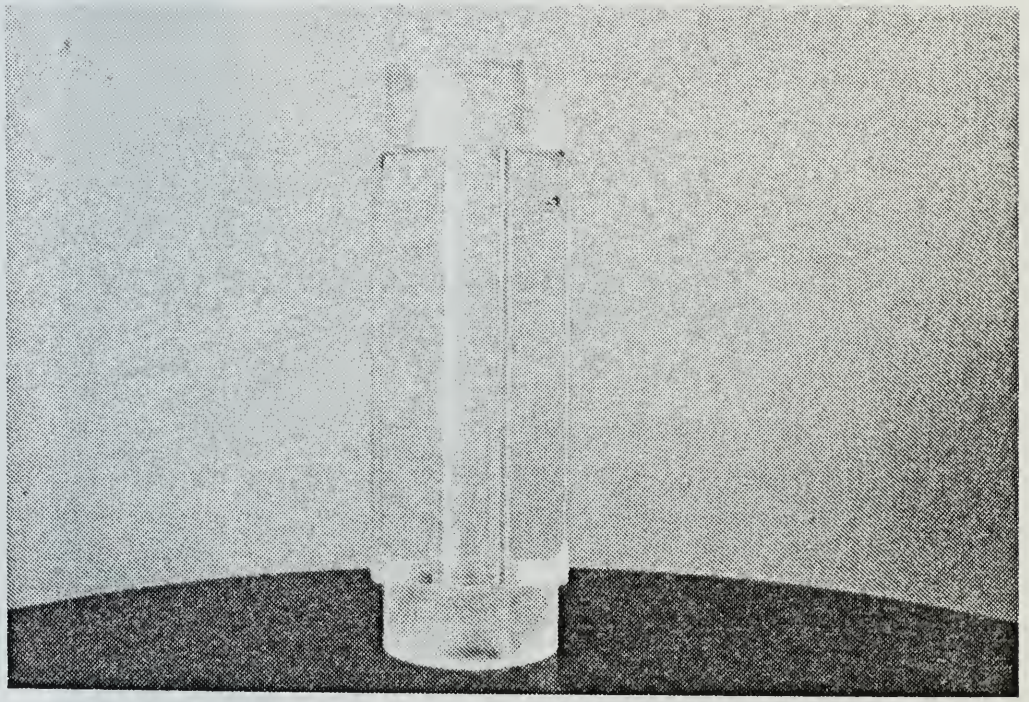

Figure 5. Photograph of Cylindrically Perforated Fuel Grain

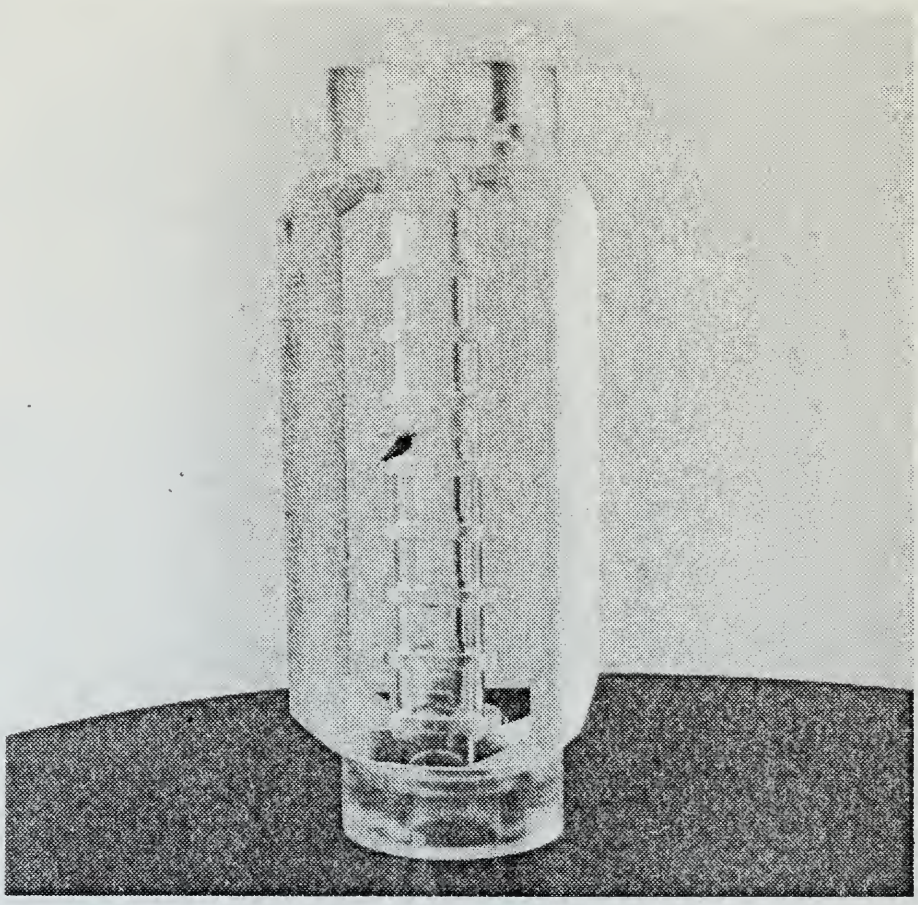

Figure 6. Photograph of Cylindrically Perforated Fuel Grain With Circumferential Grooves

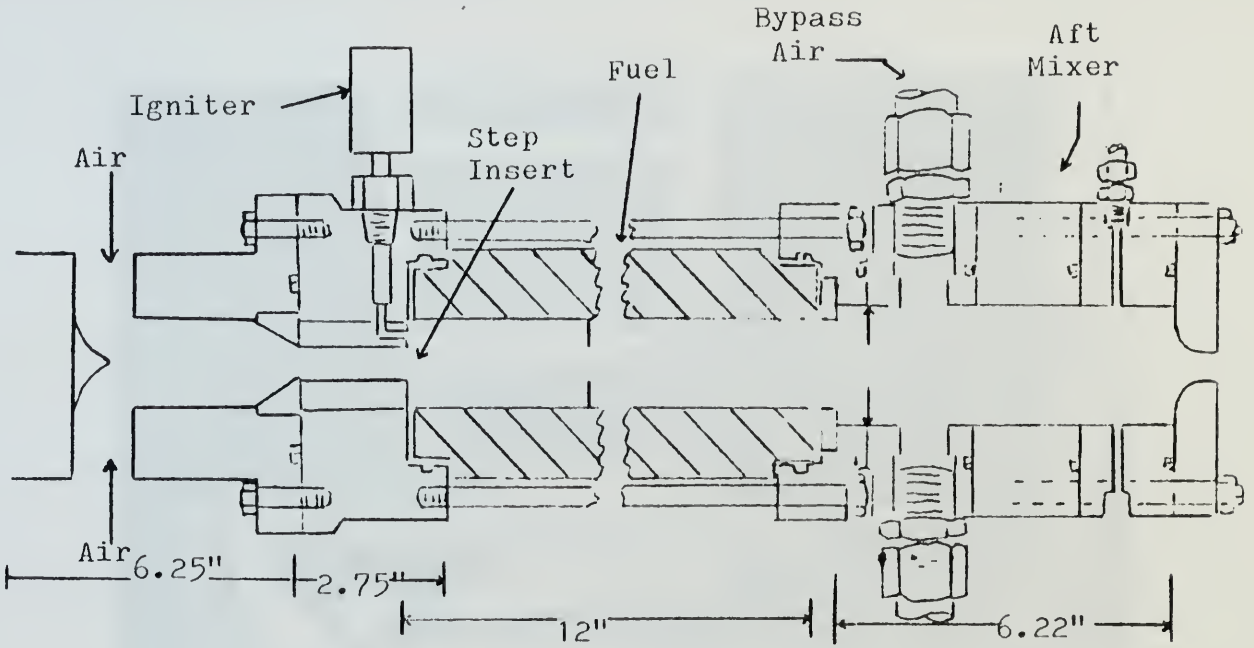

Figure 7. Schematic of Solid Fuel Ramjet Assembly

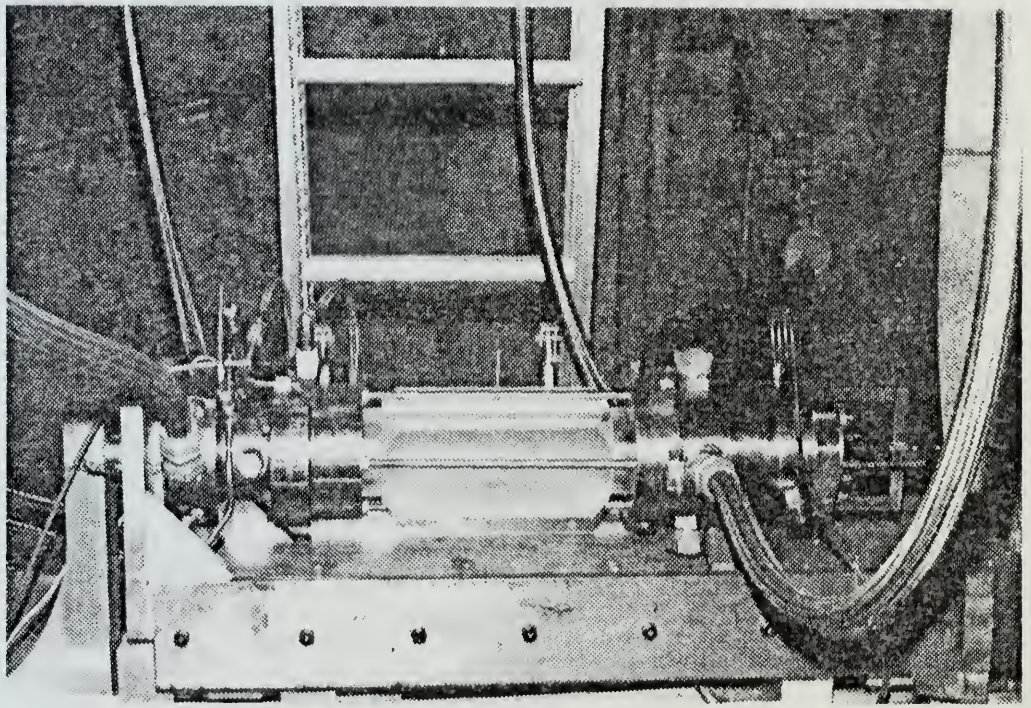

Figure 8. Photograph of Solid Fuel Ramjet Assembly

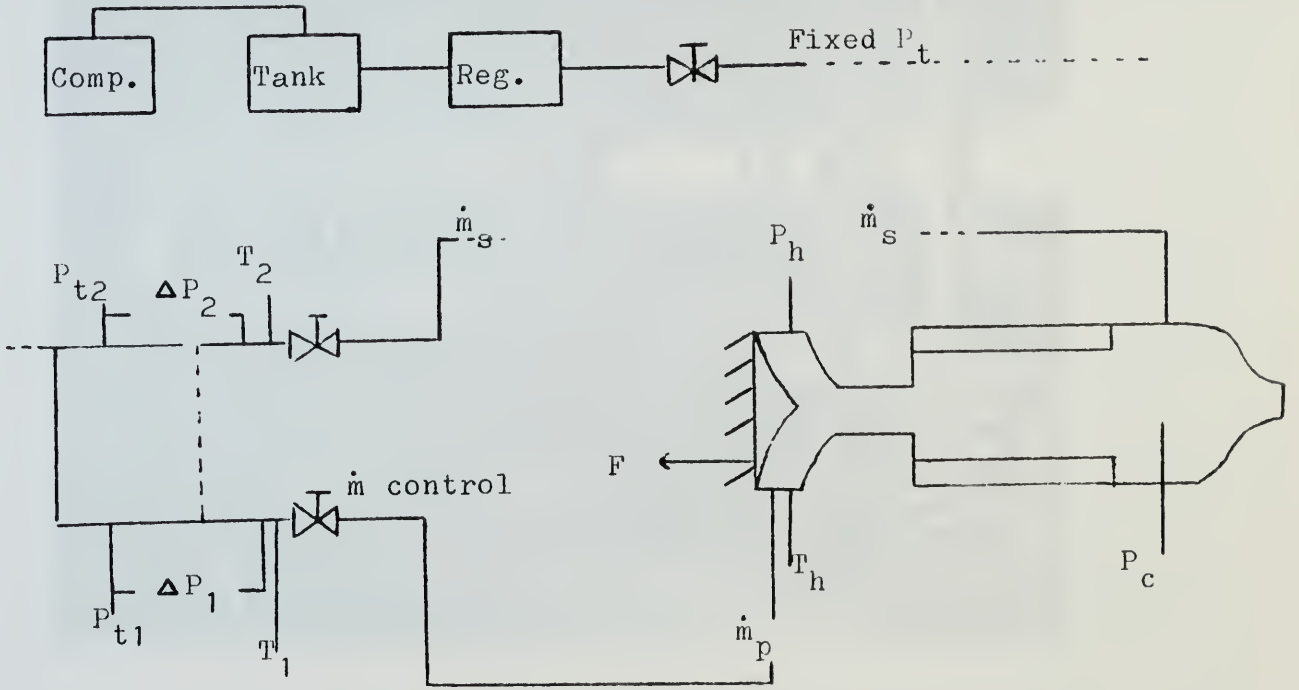

Figure 9. Schematic of Air Supply System

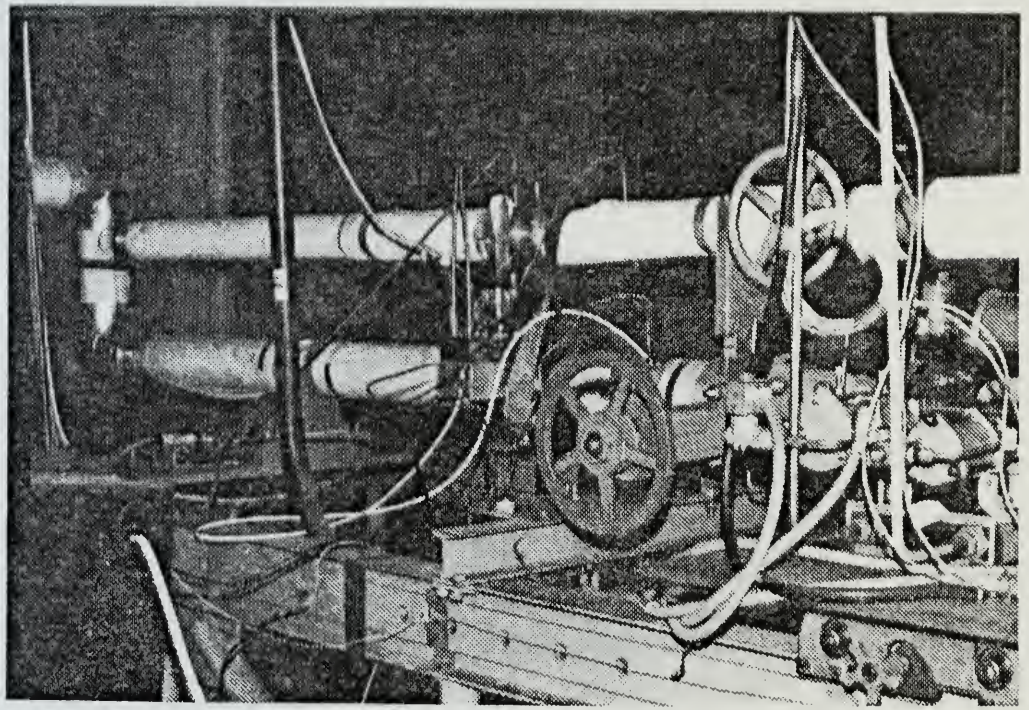

Figure 10. Photograph of Air Supply System (Controlling Gate Valves)

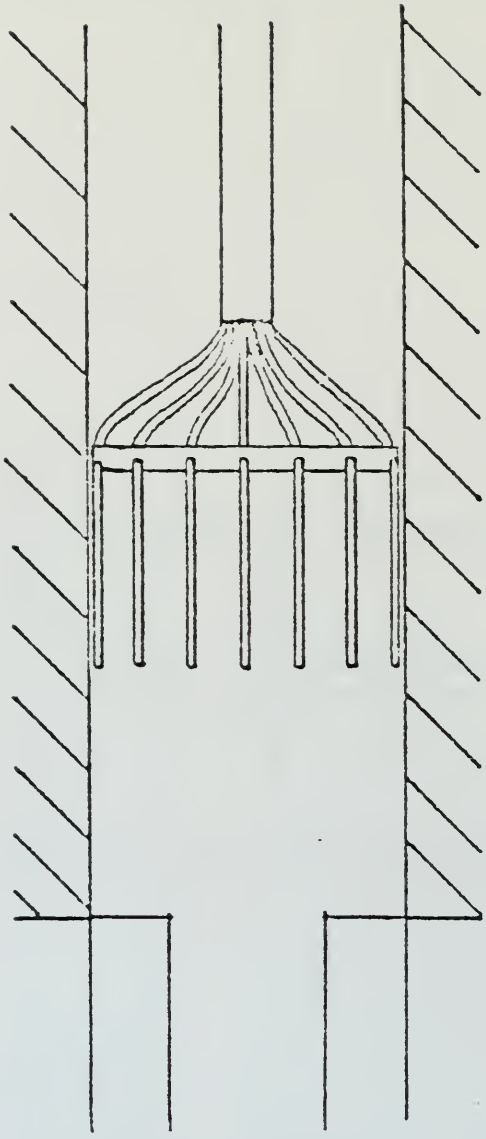

Figure 11. Schematic of Total Pressure Rake

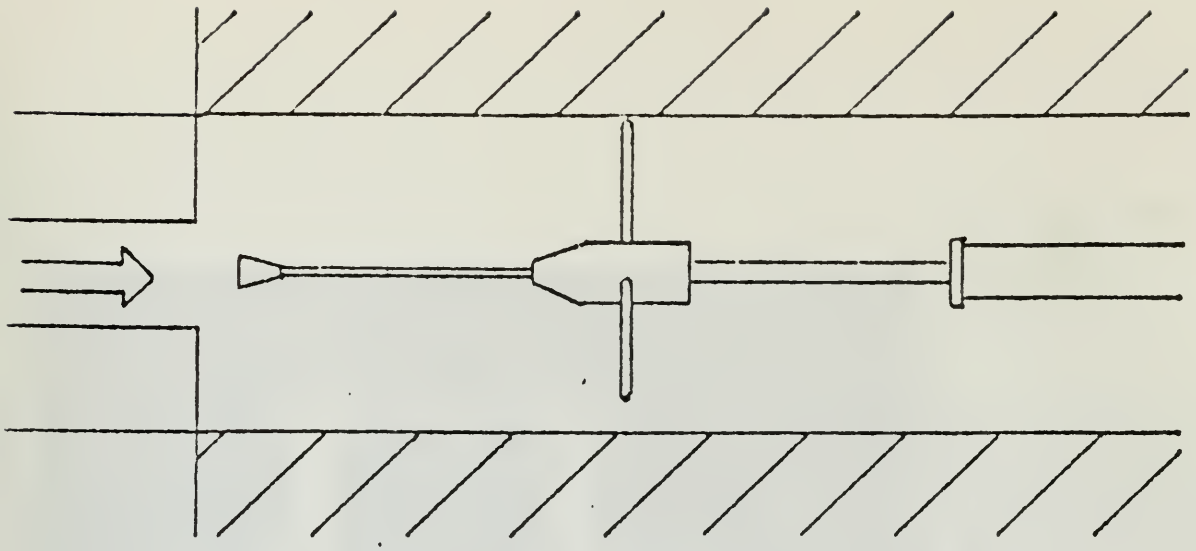

(a) Centerline Hot Wire Probe

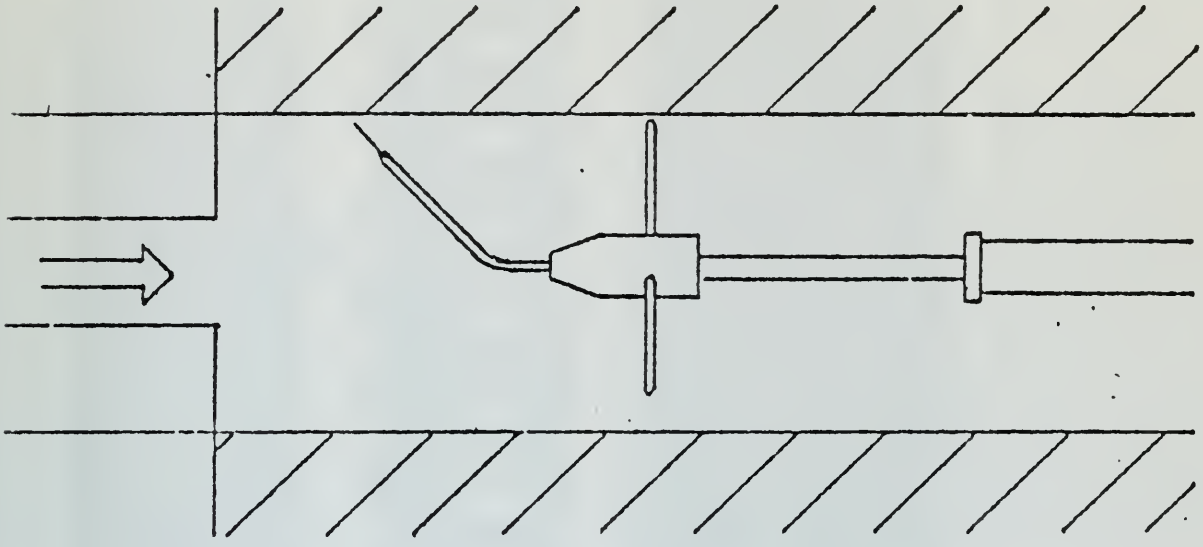

(b) Near-Wall Hot Wire Probe

Figure 12. Schematic of Hot Wire Probes

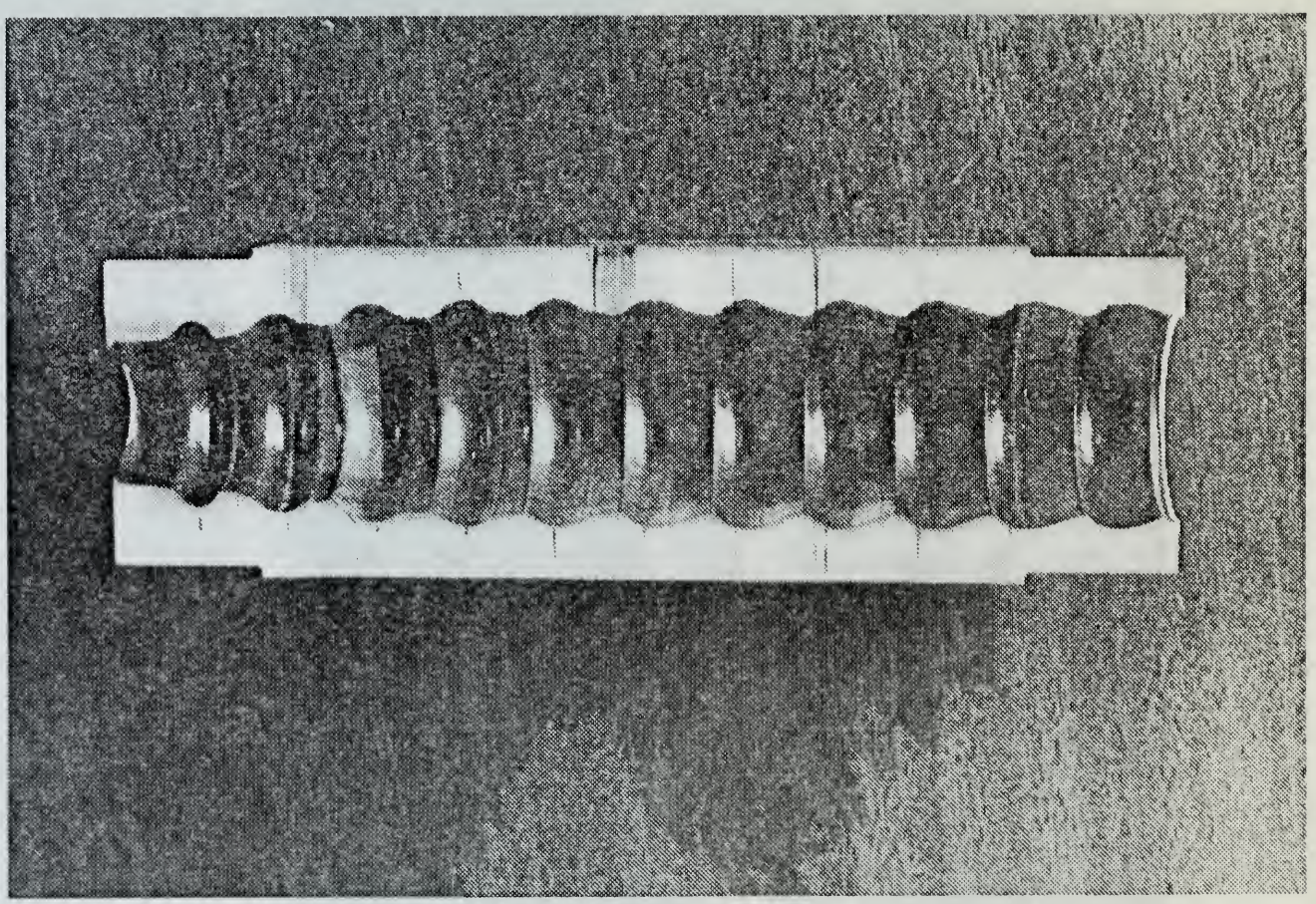

Figure 13. Photograph of Regression Pattern Inside Spent Circumferentially Grooved Fuel Grain

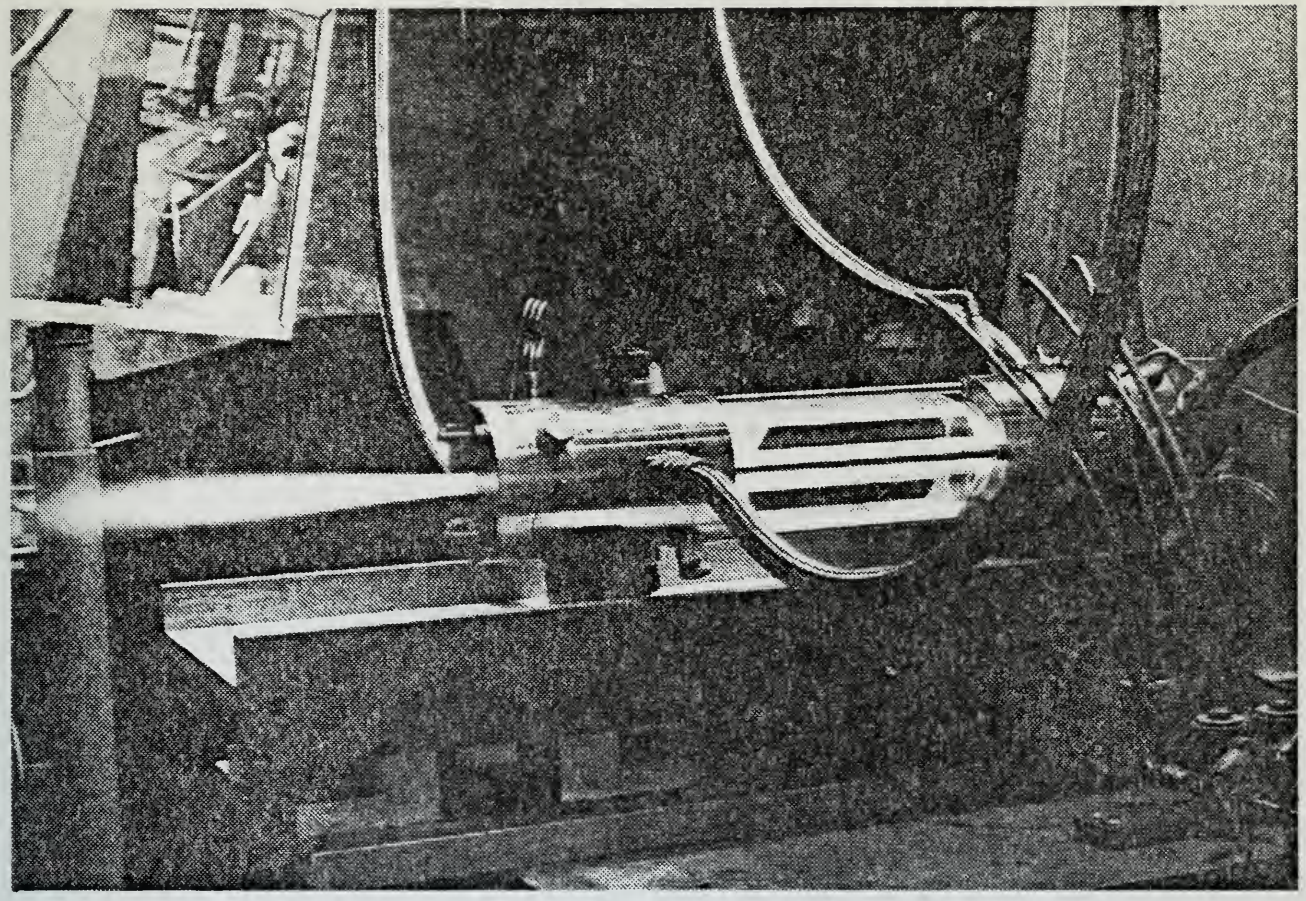

Figure 14. Photograph of Ramjet During Operation

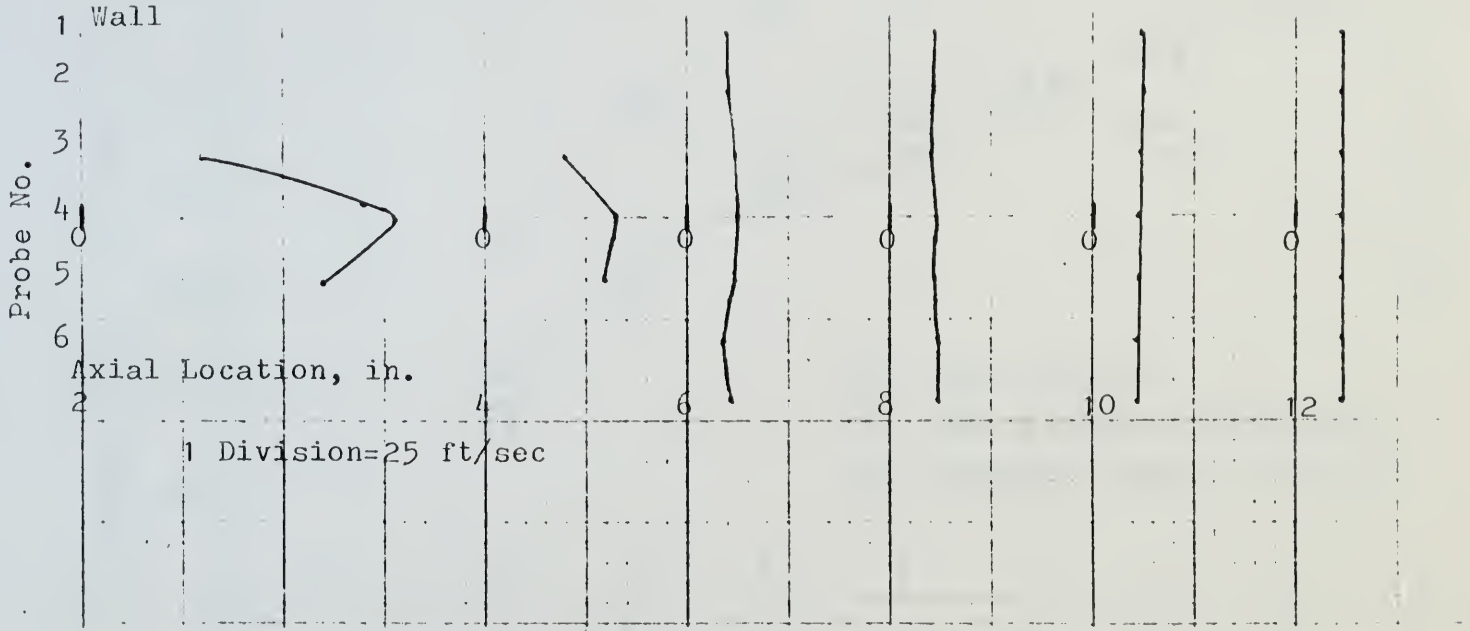

Figure 15. Velocity Profiles, Cylindrically Perforated Fuel Grain Without Bypass

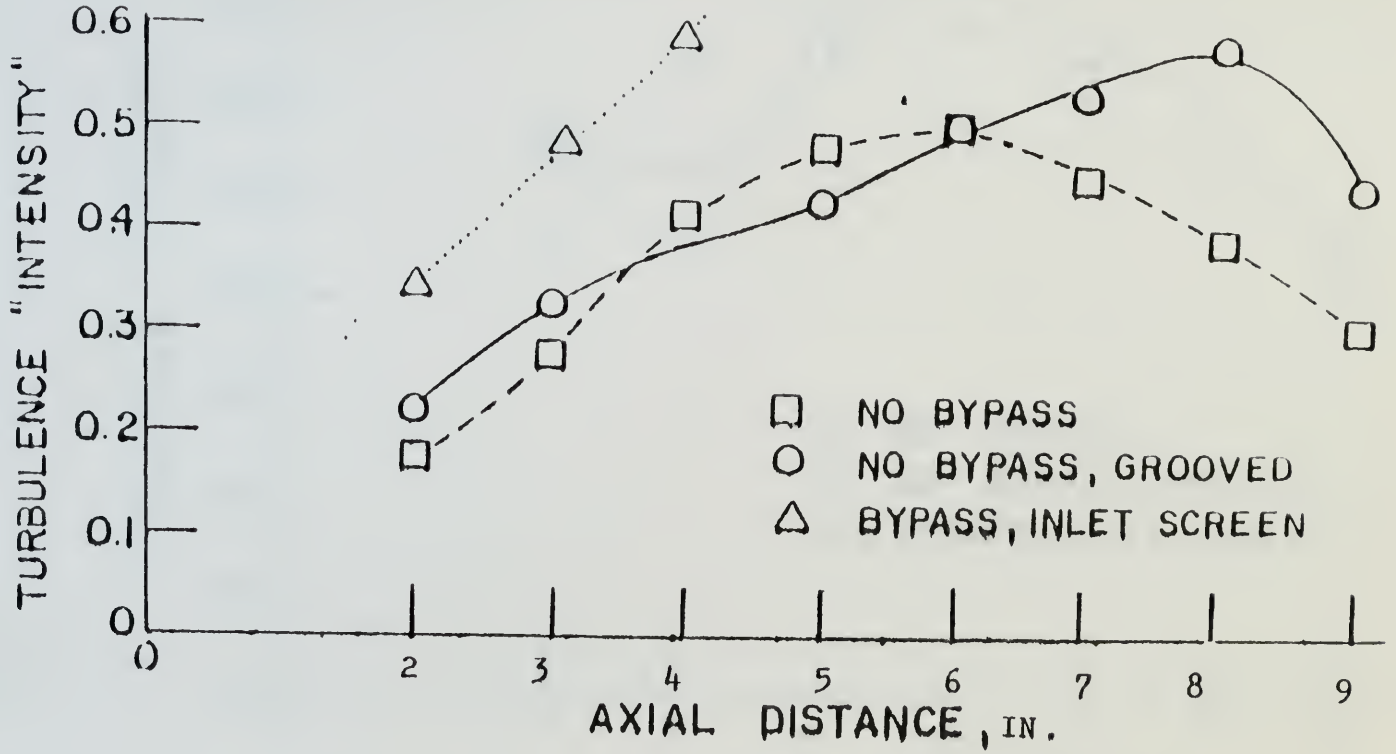

Figure 16. Centerline "Turbulence Intensity" Profiles

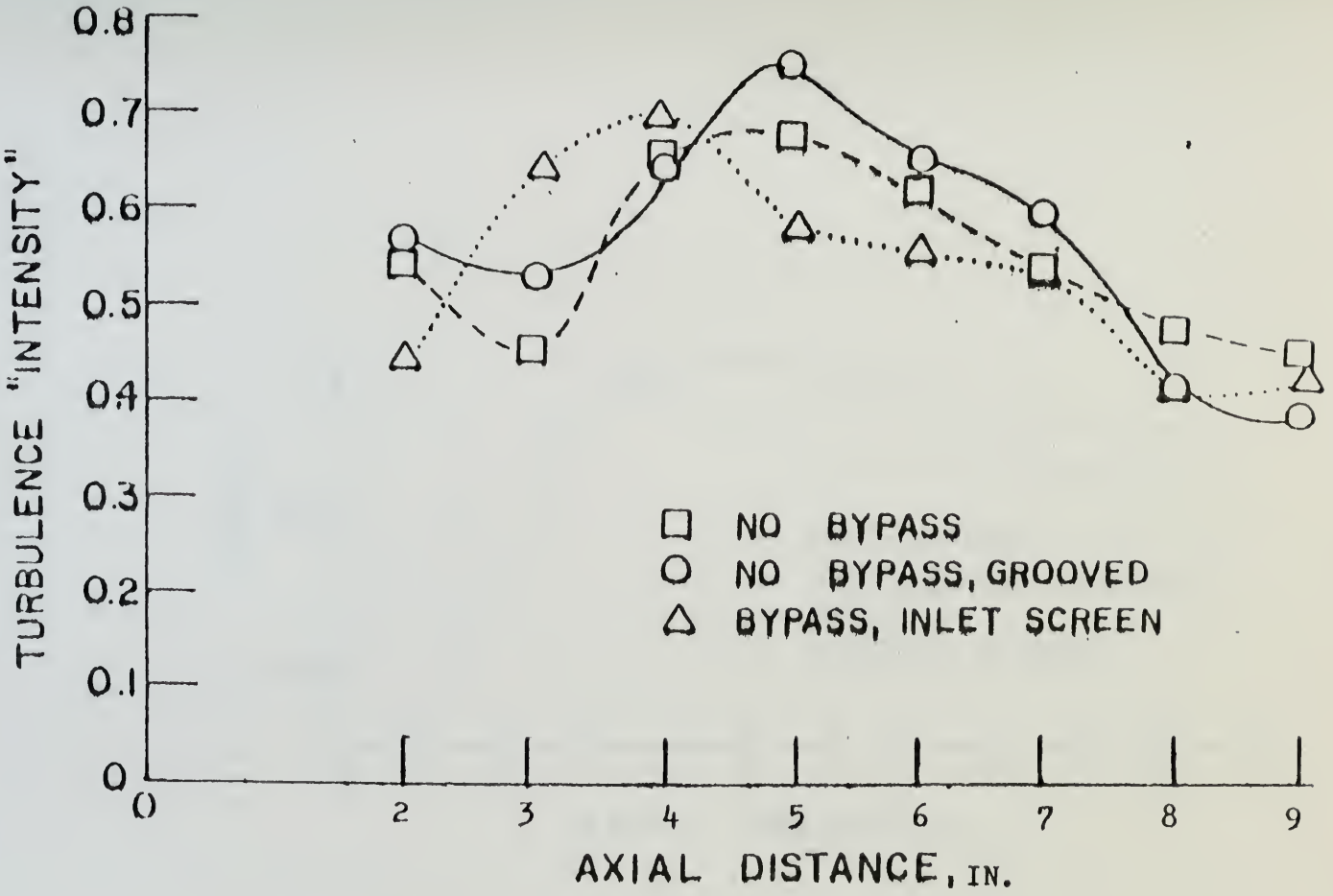

Figure 17. Near-Wall "Turbulence Intensity" Profiles

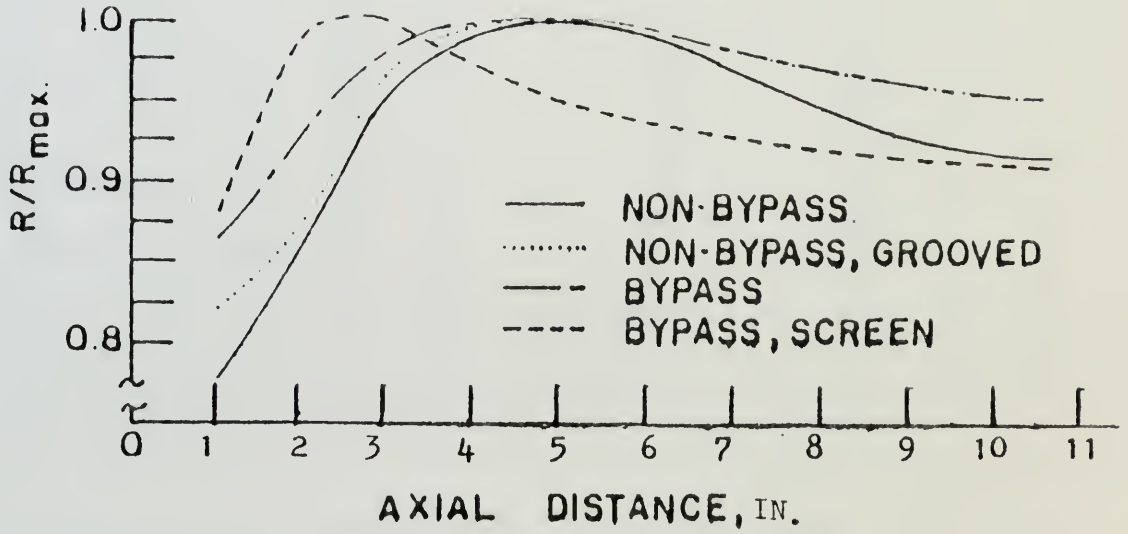

Figure 18. Fuel Regression Rate Profiles

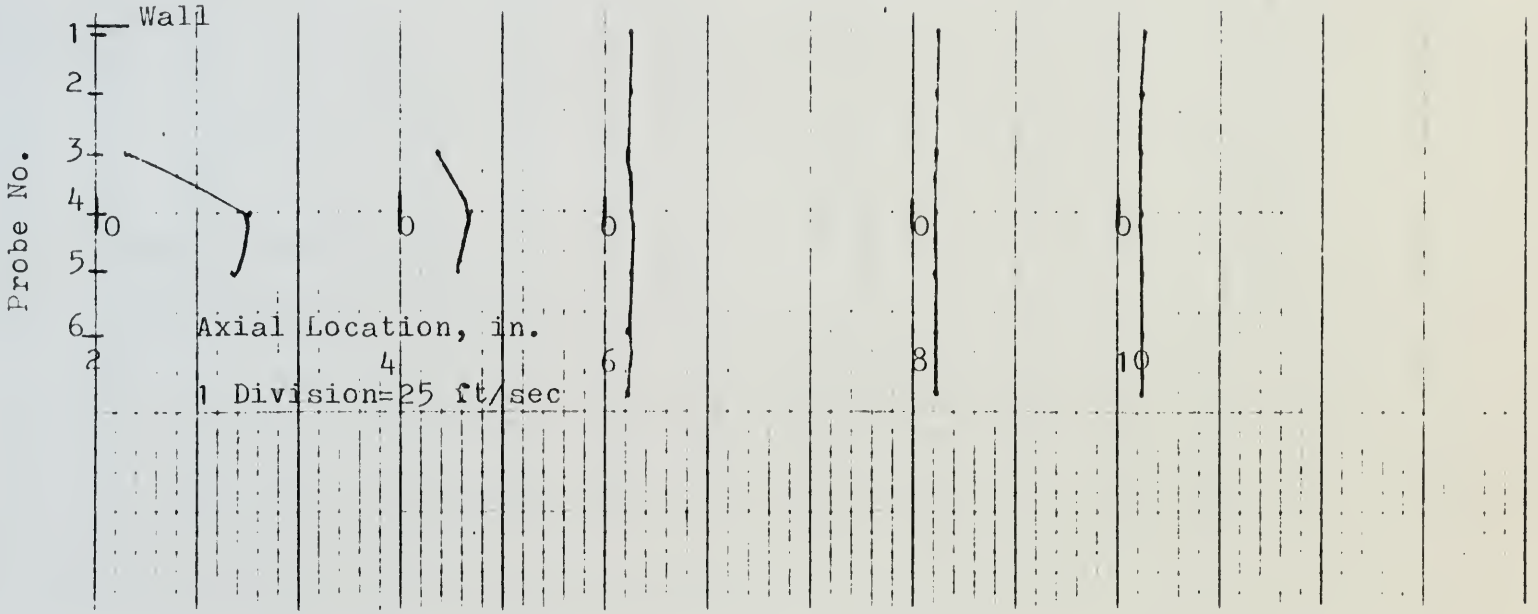

Figure 19. Velocity Profiles, Cylindrically Perforated Fuel Grain With Bypass

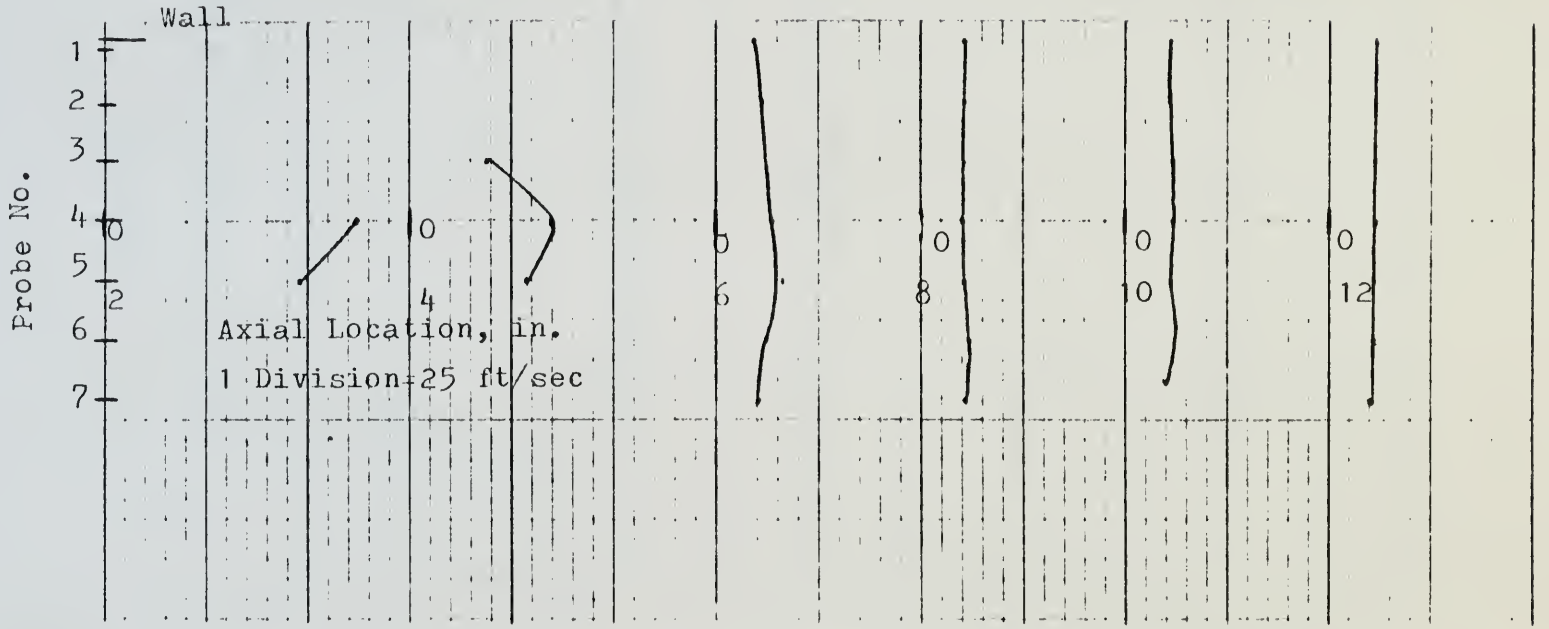

Figure 20. Velocity Profiles, Cylindrically Perforated Fuel Grain With Circumferential Grooves

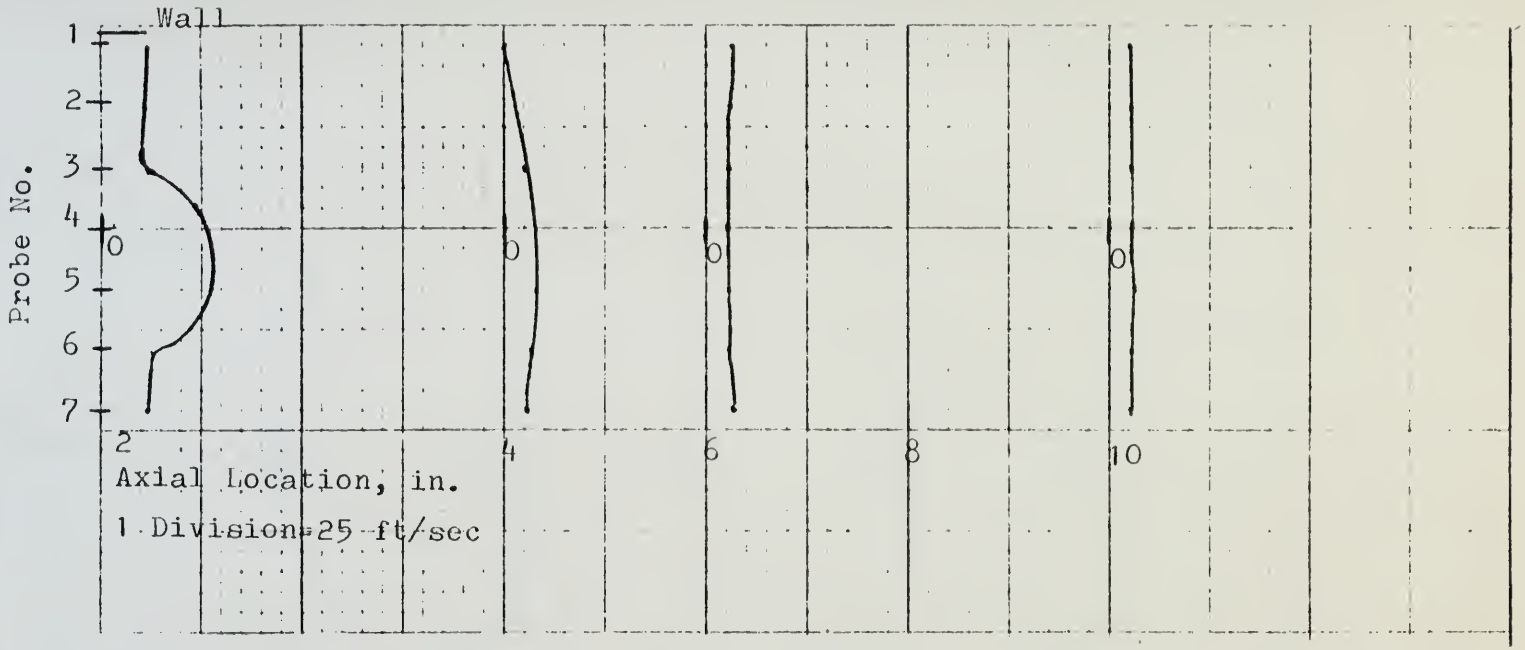

Figure 21. Velocity Profiles, Cylindrically Perforated Fuel Grain With Inlet Screen

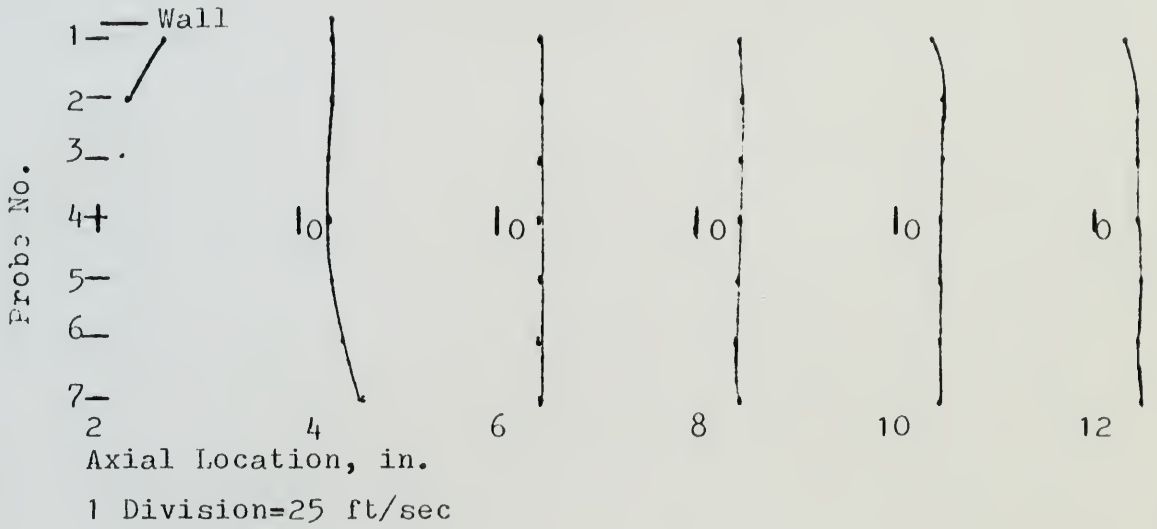

Figure 22. Velocity Profiles In-Plane of Inlet, Cylindrically Perforated Fuel Grain With Side-Dump/Dome Inlet

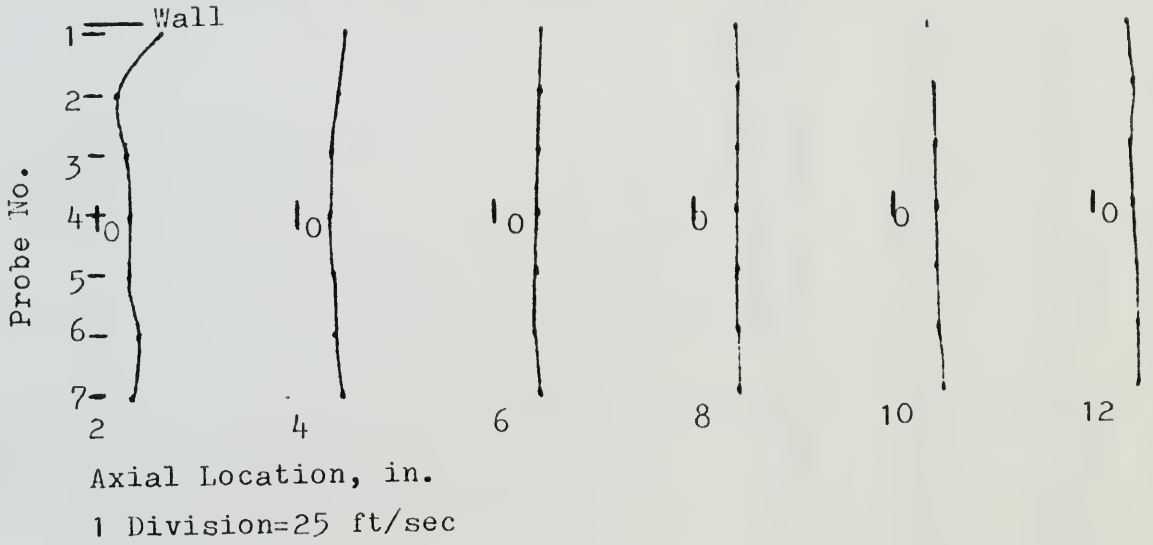

Figure 23. Velocity Profiles 90 Degrees to Inlet, Cylindrically Perforated Fuel Grain With Side-Dump/Dome Inlet

REFERENCES

1. Binn, B. A., A Comparison of Solid Fuel Ramjet Flow Characteristics and Combustion Behavior, Master's Thesis, Naval Postgraduate School, Monterey, California, 1979.

2. Flow Measurement-Supplement to Power Test Codes, v. 19.5;4, The American Society of Mechanical Engineers, 1959.

3. Naval Postgraduate School Report 57NT73031A, An Investigation of the Internal Ballistics of Solid Fuel Ramjets, by L. D. Boaz and D. W. Netzer, March 1973.

4. Naval Postgraduate School Report 67NT77092, An Investigation of the Combustion Behavior of Solid Fuel Ramjets, by C. J. Mady, P. H. Hickey, and D. W. Netzer, September 1977.

5. Naval Postgraduate School Report 57NT74081, Flow Characteristics In Solid Fuel Ramjets, by J. T. Phaneuf, and D. W. Netzer, July 1974.

INITIAL DISTRIBUTION LIST

		No. Copies
1.	Defense Technical Information Center Cameron Station Alexandria, Virginia 22314	2
2.	Library, Code 0142 Naval Postgraduate School Monterey, California 93940	2
3.	Department Chairman, Code 67 Department of Aeronautics Naval Postgraduate School Monterey, California 93940	1
4.	Assoc. Prof. D. W. Netzer, Code 67Nt Department of Aeronatics Naval Postgraduate School Monterey, California 93940	2
5.	LT Winston E. Scott 5340 Angus Virginia Beach, Virginia 23464	2

190390

Thesis
S4025 Scott
c.1 An investigation of the reacting and non-reacting flow characteristics of solid fuel ramjets.

AUG 19 85 29498

Thesis 190390
S4025 Scott
c.1 An investigation of the reacting and non-reacting flow characteristics of solid fuel ramjets.

thesS4025
An investigation of the reacting and non
3 2768 001 93347 6
DUDLEY KNOX LIBRARY